공학석사 학위논문

Mechanisms of sorption and photocatalytic degradation of clofibric acid in Fe-based Metal Organic Frameworks (MOFs)

철 기반 금속유기골격체를 이용한
clofibric acid의 흡착 및 광분해 기작

2021년 8월

서울대학교 대학원
건설환경공학부
채 승 희

Mechanisms of sorption and photocatalytic degradation of clofibric acid in Fe-based Metal Organic Frameworks (MOFs)

철 기반 금속유기골격체를 이용한
clofibric acid의 흡착 및 광분해 기작

지도교수 남 경 필

이 논문을 공학석사 학위논문으로 제출함
2021년 8월

서울대학교 대학원
건설환경공학부
채 승 희

채승희의 공학석사 학위논문을 인준함
2021년 8월

위 원 장 최용주
부위원장 남경필
위 원 최정권

Abstract

Mechanisms of sorption and photocatalytic degradation of clofibric acid in Fe-based Metal Organic Frameworks (MOFs)

Seung Hee Chae
Civil and Environmental Engineering
The Graduate School
Seoul National University

Pharmaceutical and personal care products (PPCPs) are of emerging concern having been ubiquitously detected but not fully understood of their harmful effects. Yet, no clear treatment method for their removal from water bodies have been discovered. One potential treatment of them is the usage of a simultaneous sorbent and photocatalyst. By sorbing and then degrading the pollutants through photocatalytic activity, it is viewed as efficient, economic and effective. Metal organic frameworks (MOFs) were suggested as novel materials for this purpose. However, the detailed mechanisms both for the sorption and the photocatalytic degradation process was not explicated by the past studies. Hence, in this study, the specific mechanisms were outlined by using Fe-based MOFs, MIL-101(Fe) and MIL-101(Fe)-NH_2, targeting for the removal of clofibric acid. As a result, the presence of the amine functional

group of MIL-101(Fe)-NH_2 altered the sorption and photocatalytic activities toward clofibric acid.

Physiochemical properties of MIL-101(Fe) and MIL-101(Fe)-NH_2 were analyzed using FE-SEM, XRD, and FT-IR. Both MOFs exhibited octahedral crystalline shape having functional groups including carboxylic group and amine group. Furthermore, both MOFs had large BET surface areas of 1006 and 848 m^2/g, respectively, indicating sufficient potential to be used as sorbents.

When using MIL-101(Fe) and MIL-101(Fe)-NH_2 as sorbents for clofibric acid, both exhibited high sorption efficiency but through different sorption mechanisms. MIL-101(Fe)-NH_2 sorbed clofibric acid through strong acid-base interaction between its surface amine group and the carboxyl group of clofibric acid molecule. Whereas, MIL-101(Fe) sorbed clofibric acid through pi-pi interaction. Moreover, sorption of clofibric acid on MIL-101(Fe)-NH_2 was in the form of adsorption showing limited sorption capacity when the initial concentration of clofibric acid was higher than 100 mg/L. In comparison, clofibric acid also sorbed onto the pores of MIL-101(Fe) exhibiting increased sorption capacity with the increased initial concentration of clofibric acid. pH also influenced the sorption mechanism as electrostatic interaction between the amine group of MIL-101(Fe)-NH_2 and the carboxyl group of clofibric acid was the key mechanism in between the pH of 3.18 to 4.5. Therefore, sorption efficiency was highest at pH 4.

Under visible light, clofibric acid was photocatalytically oxidized when MIL-101(Fe) was present in the solution, but almost no photocatalytic degradation was observed when MIL-101(Fe)-NH_2 was present. Throughout the reaction the formation of 4-

chlorophenol indicated that clofibric acid was indeed oxidized through photocatalytic activities of MOFs. The bandgap structure of two MOFs led to the different photocatalytic potential of MIL-101(Fe) and MIL-101(Fe)-NH_2. By calculating the energy levels of the bandgap structure, MIL-101(Fe) was capable of producing Reactive Oxygen Species, whereas MIL-101(Fe)-NH_2 could not. Specifically, MIL-101(Fe) had the conduction band energy level of -0.33 eV higher than that of needed to reduce oxygen into superoxide anion. Hence, the excited electron led to the reduction of oxygen producing superoxide anion. Superoxide anion could be further react with water molecules to from hydroxyl radicals. Therefore, through the photocatalytic activity of MIL-101(Fe), hydroxyl radical could oxidize both the sorbed and aqueous clofibric acid molecules and the hole in the valence band could also directly oxidized the sorbed species. In comparison, the conduction band of MIL-101(Fe)-NH_2 had lower potential than the oxygen reduction potential. Hence, direct oxidation by the hole in the valence band was the only pathway the clofibric acid could be oxidized. EPR results further confirmed the formation of hydroxyl radical when MIL-101(Fe) was irradiated with visible light.

Based on this research, the mechanisms of the sorption and photocatalytic degradation of clofibric acid using MIL-101(Fe) and MIL-101(Fe)-NH_2 were expounded. These findings would be helpful in developing novel methods to remove PPCPs from the wastewater by using renewable energy such as light energy.

Keywords : Metal organic framework, Pharmaceutical and personal care product, sorption, photocatalytic degradation
Student Number : 2019-24759

Table of Contents

Contents of Tables

Contents of Figures

1. Introduction

1.1 Background

1.1.1 Clofibric acid

Clofibric acid is one of pharmaceutical and personal care products (PPCPs). PPCPs refer to group of chemicals that are commonly used in the living sector. After its usage, the remaining chemicals are usually disposed through waste water. In waste water treatments, some of these chemicals are not entirely removed or degraded being disposed to natural water bodies afterward. Once these chemicals enter water bodies in nature, it is known to exhibit potential threat towards living organisms. The biggest problem regarding PPCPs is that it has not yet been entirely understood. The potential effects posed upon organisms are not clear but just known to have

there is no clear renown effect posed upon organisms. Also, no clear regulation levels of PPCPs are established by the governments. However, due to its universal usage, PPCPs are omnipresent and forcing the governments of all nations to solve this emerging concern (Nie et al., 2014).

As one of the chemical compounds belonging to PPCP groups, clofibric acid is also a contaminant that is found universally but has no clear treatment method. It is a metabolite of drug clofibrate but more frequently detected than clofibrate in water bodies (Chen et al., 2017; Gao et al., 2017). If used as a drug, it exhibits anticholesteremic and antilipemic effects. Additionally, it can be

used as herbicides. Its toxicity has not been clearly defined but it is known to have potential as an endocrine disrupting substance. Since it is widely consumed as anticholesteremic drug, it is detected ubiquitously in waste water and surface water. According to Lapworth et al., [2012], it was detected at nano-level concentrations in surface water, highest being 670 ng/L. Therefore, there is a need to clarify the treatment method to remove clofibric acid from water bodies.

Figure 1.1 shows the molecular structure clofibric acid. It is composed of one benzene ring with two functional groups attached to the ring in para positions. There is a carboxylic group at the end of one of the functional groups. Hence, clofibric acid takes pH-dependent forms since the pKa of clofibric acid is 3.18. At lower pH than the pKa, it is neutrally charged but at higher pH than the pKa, hydrogen ion is detached from the carboxylic group to be negatively charged.

Clofibric acid was selected as the reference substance for PPCPs and its sorption and photocatalytic degradation was investigated throughout this study.

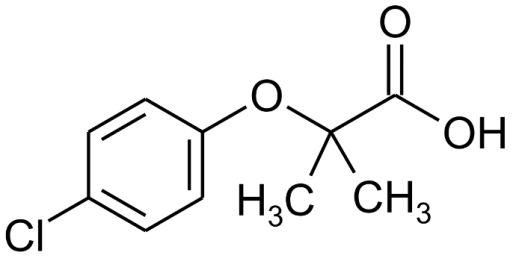

Figure. 1.1 Molecular structure of clofibric acid

1.1.2 Fe-based Metal Organic Framework (MOF)

Metal Organic Framework (MOF) refers to the crystalline porous crystalline material that is constituted by coordination bonds between metal ions or cluster and organic ligands. Organic ligands used to construct MOF has more than two coordination bonding sites in order to connect different metal clusters forming a crystal shape. Stemming from the cage shape of the crystal, MOFs usually possess high surface area. Also, based on the type of the metal and organic ligand, it can be utilized as sorbents, catalysts, and batteries (Hasan & Jhung, 2015; Y. C. He et al., 2015; Shen et al., 2016).

Out of various MOFs, Fe-based MOFs is group of MOFs having iron as the center metal. The type of Fe-based MOFs differs depending on what kind of organic ligand was used to synthesize the material. Among various Fe-based MOFs, MIL-101(Fe) and MIL-101(Fe)-NH_2 were selected as the reference MOF material in this study. Organic ligands of MIL-101(Fe) and MIL-101(Fe)-NH_2 are terephthalic acid (BDC) and 2-aminoterephthalic acid (2ATA), respectively. As seen from Figure 1.2, both organic ligands have two carboxylic groups oppositely attached to a benzene ring. These carboxylic groups serve as coordination sites with iron. As hydrogen ion is detached from the carboxylic group, two outlying oxygens are capable to form coordination bonds with two different iron ions. Again, the other two oxygens from the opposite carboxylic group form coordination bonds with additional two different iron ions. Hence, one organic linker can link four different iron ions. From the point of view of the iron ion, trivalent iron (Fe(III)) can form six coordination bonds.

Out of these six sites, only four sites are taken up by four different organic ligands. The other site is taken by oxygen and this oxygen is shared by three other iron ions. The last site forms coordination bond with chlorine or water molecules. Hence, the three iron molecules sharing the same oxygen ion is defined as the secondary building unit of MIL-101(Fe) and MIL-101(Fe)-NH_2. The only difference between MIL-101(Fe) and MIL-101(Fe)-NH_2 is the additional functional group attached on to the benzene ring.

Figure. 1.2. Organic ligands used in MIL-101(Fe) (left) and MIL-101(Fe)-NH_2 (right)

MIL-101(Fe) and MIL-101(Fe)-NH_2 is known to show less toxicity compared to the other MOFs that use various heavy metals as central ions(Bezverkhyy et al., 2016; Gao et al., 2017; Horiuchi et al., 2016). Also, like other MOFs, they are known to have very high specific surface area. Furthermore, there may be unsaturated sites in the iron ion which can contribute as sorption sites of other molecules (Hasan et al., 2013). Moreover, they are known to possess semiconductor properties which can enable Fenton process in water to form free radicals. Especially, the Fe_3-μ_3-oxo cluster is known to be responsible for the absorption of visible light (Horiuchi et al., 2016; Z. Zhang et al., 2016).

In this study, MIL-101(Fe) and MIL-101(Fe)-NH_2 were selected both as a sorbent and photocatalyst that can remove clofibric acid from water bodies.

1.2 Literature review

Past studies have reported the possibility of Fe-based MOFs including MIL-101(Fe) and MIL-101(Fe)-NH_2 to be utilized as sorbents or photocatalysts. Dong et al., [2020] utilized MIL-101(Fe) and MIL-101(Fe)-NH_2 as sorbents for tetracycline. Both MOFs were synthesized via microwave-assisted method leading to smaller particle size of particles. With the increased higher specific surface area, both MOFs exhibited high adsorption capacity of tetracycline in wastewater. MIL-101(Fe)-NH_2 showed higher adsorption capacity than MIL-101(Fe) through electrostatic interaction whereas, MIL-101(Fe) adsorbed tetracycline molecules through pi-pi stacking interaction.

J. He et al., [2018] utilized MIL-88B(Fe)-NH_2 for the removal of methylene blue through sorption. The electrostatic interaction and acid-base interaction between the functional groups of two materials was the main mechanism for the removal. Furthermore, this study also investigated the Fenton activities of MOFs by adding H_2O_2. In result, MIL-88B(Fe)-NH_2 was capable of producing hydroxyl radicals, degrading the adsorbed methylene blue molecules.

C. Zhang et al., [2015] utilized MIL-101(Fe)-NH_2 as a photocatalyst for the removal of toluene gas molecules. Xenon lamp was selected as the light source of this research indicating that MIL-101(Fe)-NH_2 was indeed possible to utilize visible light. Moreover, Laurier et al., [2013] compared the photocatalytic activity of different Fe-based MOFs, MIL-100(Fe), MIL-88B(Fe), MIL-88B(Fe)-NH_2, and MIL-101(Fe)-NH_2 with the target

pollutant as rhodamine 6G. The light source of this research was monochrome with two different wavelengths of 350, and 550 nm. With the monochromatic light source, MIL-88B(Fe) showed the highest removal Lastly, Wang et al., [2018] utilized three Fe-based MOFs, MIL-100(Fe), MIL-53(Fe), and MIL-101(Fe) as photocatalysts for the removal of tetracycline. Xenon lamp was once more utilized as the light source. The results indicated that out of the three Fe-based MOFs, MIL-101(Fe) showed the highest photocatalytic activity.

From the past studies, it can be inferred that Fe-based MOFs are capable to serve both as sorbents and photocatalysts. However, one of the limitations of the past research was that they assumed that the removal of contaminants in the aqueous phase was due to the photocatalytic degradation excluding the possibility of additional sorption of the pollutant. Therefore, in this study, the sorbed species during photocatalytic degradation reaction were also into consideration and were analyzed. By calculating the sorbed amount of the pollutant, differentiation between photocatalytic degradation and sorption became possible.

1.3 Research objective

The objective of this research is to investigate the removal mechanisms of clofibric acid through the sorption and photocatalytic degradation by MIL-101(Fe) and MIL-101(Fe)-NH_2. Especially, the presence of amine group was accounted for the difference between MIL-101(Fe) and MIL-101(Fe)-NH_2 towards sorption and photocatalytic activity. In order to achieve this objective, the study was carried out in three following steps.

(1) Physiochemically characterizing MIL-101(Fe) and MIL-101(Fe)-NH_2 in order to determine whether they were fabricated successfully. Additionally, the purpose of this step is to estimate their potential for sorption of clofibric acid.

(2) Determining the sorption mechanism of clofibric acid towards MIL-101(Fe) and MIL-101(Fe)-NH_2. The affect of pH should be included in this step in order to elucidate the interaction between the amine group of MIL-101(Fe)-NH_2 and clofibric acid.

(3) Determining the photocatalytic degradation of clofibric acid using MIL-101(Fe) and MIL-101(Fe)-NH_2. The photocatalytic degradation pathway of clofibric acid and the photocatalytic characteristics of MIL-101(Fe) and MIL-101(Fe)-NH_2 should be explicated to fully explain the photocatalytic degradation mechanism.

2. Materials and method

2.1 Materials

Iron(III) chloride hexahyrate (97%, Sigma-Aldrich), terephthalic acid (99%, Junsei), and 2-aminoterephthalic acid (98%, TCI) were used to synthesize two Fe-based MOFs, MIL-101(Fe) and MIL-101(Fe)-NH_2. Acetonitrile (99.8%, Daejung), ethyl alcohol, anhydrous (99.9%, Daejung), N,N-Dimethylformamide (99.5%, Daejung), hydrofluoric acid (48.0-51.0%, J. T. Baker), and methyl alcohol (99.9%, Daejung) were used as organic solvents through out the research. Additionally, hydrochloric acid (35%, Daejung), and sodium hydroxide beads (97%, Daejung) were used during sorption and photocatalytic degradation experiments to adjust pH. The targeted pollutant in this research was 2-(4-Chlorophenoxy)isobutyric acid (clofibric acid) (97%, TCI).

2.2 Synthesis of Fe-based MOFs

Two kinds of Fe-based MOFs, MIL-101(Fe) and MIL-101(Fe)-NH_2, were synthesized and used in this research. MIL-101(Fe) was synthesized using the microwave-heating method, whereas MIL-101(Fe)-NH_2 was synthesized using the solvothermal method (Horiuchi et al., 2016; Liu et al., 2019).

MIL-101(Fe) was synthesized following these steps. 1 mol of $FeCl_3 \cdot 6H_2O$ and 2 mol of terephthalic acid (BDC) was dissolved in 160 mol dimethylformamide (DMF). 20 μL of HF was added to the mixture. The final mixture was placed in teflon lined vessels which was microwaved for 20 hours at 110℃ (MSP1000, CEM, USA). Under microwave, crystalline structure of metal organic framework was formed. Afterwards, the mixture was collected using FEP conical tube. The mixture was centrifuged at 10,000 xg for 5 minutes at 4℃ to collect the solids. After discarding the supernatant, the solids were washed with hot ethanol using the oil bath at 60℃ for 6 hours. Washed solids were placed in the oven at 60℃ overnight to evaporate the remaining ethanol inside the pores.

MIL-101(Fe)-NH_2 was synthesized using the solvothermal method. 2.5 mol of $FeCl_3 \cdot 6H_2O$ and 1.2 mol of 2-amino terephthalic acid (2ATA) was dissolved in 97 mol of dimethylformamide (DMF) each. Two mixtures were combined together to form the final mixture. The mixture was placed in the Teflon lined autoclave which was then heated up to 110℃ for 24 hours. The sample collection and washing procedures were same as the procedures of MIL-101(Fe) synthesis.

2.3 Characterization of Fe-based MOFs

2.3.1 Physical properties of Fe-based MOFs

The Brunauer-Emmett-Teller (BET) surface area and pore size distribution of MIL-101(Fe) and MIL-101(Fe)-NH_2 were characterized by N_2 adsorptions patterns using (BELsorp X mini, Microtrac BEL, Japan). The samples were pretreated at 180℃ for 3 hours. After obtaining the N_2 adsorption data, BET surface area was calculated by using the analysis program BELMaster Version 7.2.0.4. Average pore size was also calculated by using the same software.

Particle size distributions of MIL-101(Fe) and MIL-101(Fe)-NH_2 were measured by using Dynamic Light Scattering Spectrophotometer (DLS-7000, Otsuka Electronics. Co., Ltd., Japan). Zeta potentials of MIL-101(Fe) and MIL-101(Fe)-NH_2 were measured by using Electrophoretic Light Scattering Spectrophotometer (ELS Z-1000, Otsuka Portal, Japan).

The shape of MIL-101(Fe) and MIL-101(Fe)-NH_2 were analyzed using Field-Emission Scanning Electron Microscope (FE-SEM) (SUPRA 55VP, Carl Zeiss, Germany). The powder sample was fixed to the holder using a piece of carbon tape. The sample was coated with Pt for 120 seconds in the power of 30 mA. The prepared sample was loaded in the device afterward.

The crystal structure of MIL-101(Fe) and MIL-101(Fe)-NH_2 were analyzed by Powder X-Ray Diffraction (PXRD) (D8 ADVANCE with DAVINCI, Bruker AXS, Germany). $CuK_{\alpha 1}$ radiation source was used to record the intensity in between 5° to 90° 2θ with the increment of 0.02° 2θ. The examined PXRD patterns of

MIL-101(Fe) and MIL-101(Fe)-NH_2 were directly compared with the simulated PXRD pattern of MIL-101(Cr). The crystalline information file (CIF) of the MIL-101(Cr) was downloaded from Crystallography Open Database (COD), having the CIF number of 4000663. With the CIF file of MIL-101(Cr), the PXRD pattern was simulated using the crystal and molecular structure visualization program, Diamond 3.2.

2.3.2 Chemical properties of Fe-based MOFs

The surface groups of MIL-101(Fe) and MIL-101(Fe)-NH_2 were also analyzed with Fourier Transform Infrared Spectroscopy (FT-IR) (Nicolet 6700, Thermo Scientific, USA). The range of the measured wavelength was 4000 to 650 cm^{-1}, with the resolution of 8 cm^{-1}. By referring to the FT-IR table, the surface functional groups of MIL-101(Fe) and MIL-101(Fe)-NH_2 were analyzed with the results.

2.4 Determination of the sorption mechanism of clofibric acid with Fe-based MOFs

2.4.1 Sorption mechanisms at various pH levels

In order to obtain the sorption kinetics and isotherms of clofibric acid using MIL-101(Fe) and MIL-101(Fe)-NH_2, the pH was set to 4.0. 40 ml of clofibric acid solution, with the initial concentrations of 25, 50, 100, 150 mg/L were placed in 50 ml conical tubes. 4 mg of MIL-101(Fe) and MIL-101(Fe)-NH_2 were put into each clofibric acid solutions. The mixture of the clofibric acid solution and Fe-based MOFs were **mixed** throughout the adsorption experiment using the conical tube rotator. 1 ml of the sample was taken from the solution at time 0, 1, 5, 10, 30, 60, and 120 minutes. Samples were filtered using the 0.22 μm PTFE syringe filter (Futecs, Korea). All experiments were triplicated.

To test the influence of pH on the sorption mechanism of clofibric acid onto MIL-101(Fe) and MIL-101(Fe)-NH_2, additional sorption tests were carried out with the pH at 3, 5, 7, 9. pH was adjusted by adding adequate amount of 0.1M NaOH and 1% HCl solution at each sampling time in order to maintain the targeted pH over the experiment period. Initial concentration of clofibric acid was all set to 50 mg/L. Other settings such as the amount of sorbent, amount of solution, and the sampling time and amount were kept the same as the original sorption experiment. All experiments were triplicated.

Clofibric acid concentration of the samples were measured by high performance liquid chromatography equipped with UV

(HPLC-UV) (YL9100, YL instrument, Korea) with a ZORBAX Eclipse Plus C18 column (4.6 x 250 mm, 5 μm). The mobile phase was a mixed solution containing an aqueous buffer (1L DI, 50 ml methanol, 4 ml phosphoric acid) and acetonitrile (v/v=4:6) with the flowrate of 1.0 ml/min. The sample injection volume was 20 μl and the detector wavelength was set to 226 nm. The temperature was set to 25℃.

After the sorption experiment, FT-IR spectrum of the MIL-101(Fe) and MIL-101(Fe)-NH_2 were analyzed. In order to obtain enough amount of solid samples of MIL-101(Fe) and MIL-101(Fe)-NH_2 for FT-IR analysis, the sorption tests were performed at a bigger scale. 200 ml of the 50 mg/L clofibric acid solution was set in the 500 ml glass beaker. To keep the same ratio of the sorbent as the original sorption experiment, 20 mg of MIL-101(Fe) and MIL-101(Fe)-NH_2 was mixed with the solution. The temperature was set to 25℃. After two hours, MIL-101(Fe) and MIL-101(Fe)-NH_2 were retrieved using vacuum filter with 0.22 μm filter (Whatman, UK). MIL-101(Fe) and MIL-101(Fe)-NH_2 were collected after drying the filters in the oven at 60℃ overnight. FT-IR was analyzed with the same equipment and settings as used for the raw MIL-101(Fe) and MIL-101(Fe)-NH_2 characterization.

After the sorption test at different pH, MIL-101(Fe) and MIL-101(Fe)-NH_2 were also retrieved for FT-IR analysis. Sorption test settings were all the same as above except the pH. pH of the samples were kept at 2, 6, and 8 over the experiment using 0.1M NaOH and 1% HCl solution. For comparison, two Fe-based MOFs were soaked in distilled water at pH4 and retrieved afterward. Again, solid samples were collected using the vacuum filter and

drying them afterwards. FT-IR analysis settings were also the same with the raw MIL-101(Fe) and MIL-101(Fe)-NH_2 characterization.

2.4.2 Sorption thermodynamic parameter

Sorption experiments were also carried out at various temperatures in order to measure the thermodynamic parameters of the sorption process of clofibric acid onto MIL-101(Fe) and MIL-101(Fe)-NH_2. Temperature of the sorption experiments were set at 25, 35, 45℃ using the rotator inside the hybridization incubator (combi-V12, FINEPCR, Korea). Initial concentrations of clofibric acid were set to 25, 50, 100, 150 mg/L. The amount of sorbent, amount of solution, and the sampling intervals and amount were kept the same as the original sorption experiment. The initial pH of the solution was set to 4 as well. The clofibric acid concentration of the samples were analyzed by using HPLC-UV as well. All experiments were triplicated.

2.5 Photocatalytic degradation of clofibric acid with Fe-based MOFs

2.5.1 Photocatalytic degradation of clofibric acid

2.5.1.1 Photolysis of clofibric acid

To eliminate the possibility that clofibric acid is degraded without the presence of photocatalyst, photolysis experiment of clofibric acid was carried out. For the light source, xenon lamp was selected with the power of 400W (XPN500WA, DY-Tech, Korea). Because xenon lamp shows similar light spectrum with the Sun, it is commonly used as the light source for visible light viable photocatalyst experiments. The lamp chamber had the dimension of 265 x 190 x 180 mm with the circular hole heading below where light could be transmitted. UV-cutoff filter was installed in front of the circular hole in order to remove the UV region (<420 nm) of the lamp. Hence, the experiment results are the outcomes by using only the visible light region of the lamp.

Initial concentration of the clofibric acid was 50 mg/L and the initial pH was set to 4. 150 ml of the clofibric acid solution was put into a 250 ml jacketed reaction vessel. The vessel was placed directly below from the lamp. The solution was stirred using the magnetic bar to help all part of the solution get equal exposure to the light. Pumps coming out from the circulating water bath (LC-LT212, LK LAB, Korea) were connected to each outlying holes of the vessel to avoid the heating of the solution due to irradiation and maintain the temperature as 25°C during the experiment. 1 ml of

samples were collected at 0, 1, 5, 10, and 30 minute time period and 1, 2, 3, 4, 5, 6, and 24 hour time period. The clofibric acid concentration of the samples were analyzed via HPLC-UV. All experiments were triplicated.

2.5.1.2 Photocatalytic degradation pathway

The influence of MIL-101(Fe) and MIL-101(Fe)-NH_2 in the photocatalytic degradation of clofibric acid was measured as follow. The lamp settings were the same as the photolysis experiment. 150 ml of the clofibric acid solution (50 mg/L, pH 4) was also put into the 250 ml jacketed vessel which was connected to the circulating water bath maintaining the temperature at 25°C. 45 mg of MIL-101(Fe) or MIL-101(Fe)-NH_2 was added to the solution. The solution was stirred using the magnetic bar. At first, the mixture was placed at dark for 30 minutes to reach the adsorption equilibrium of clofibric acid. After reaching the equilibrium, xenon lamp with the power of 400 W was vertically set to the solution.

Concentration of clofibric acid was measured in two ways. One was to measure the aqueous concentration of the clofibric acid and the second was to measure the total clofibric acid including the portion that was sorbed to MIL-101(Fe) or MIL-101(Fe)-NH_2. Both samples were collected with the volume of 0.5 ml at time period of before and after the adsorption, 1, 5, 10, and 30 minutes, 1, 2, 3, 4, 5, 6, 24 hours after setting the light on the sample. To measure the aqueous concentration of the samples, the samples were filtered using 0.22 μm PTFE syringe filter and were directly analyzed using HPLC-UV.

At extremely high pH conditions (pH > 11), the structures of MIL-101(Fe) and MIL-101(Fe)-NH_2 were destroyed. This was due to the breakage of the coordination bond between iron and organic linkers to form ferrihydrite ($Fe(OH)_3$). The formation of ferrihydrite was proved through analyzing the precipitated solids with XRD. The XRD patterns of the solids are shown in Figure. 2.1. Since clofibric acid was not sorbed to ferrihydrite nor destroyed during the procedure, the sorbed fraction of clofibric acid onto MIL-101(Fe) and MIL-101(Fe)-NH_2 could be detached easily by increasing the pH of the solution. Therefore, to measure the total concentration of clofibric acid, 0.5 ml of the solution sample was mixed with 1 ml of 10^{-3} M NaOH solution and then was filtered with 0.22 μm PTFE syringe filter. The concentration was analyzed by HPLC-UV as well. All experiments were triplicated.

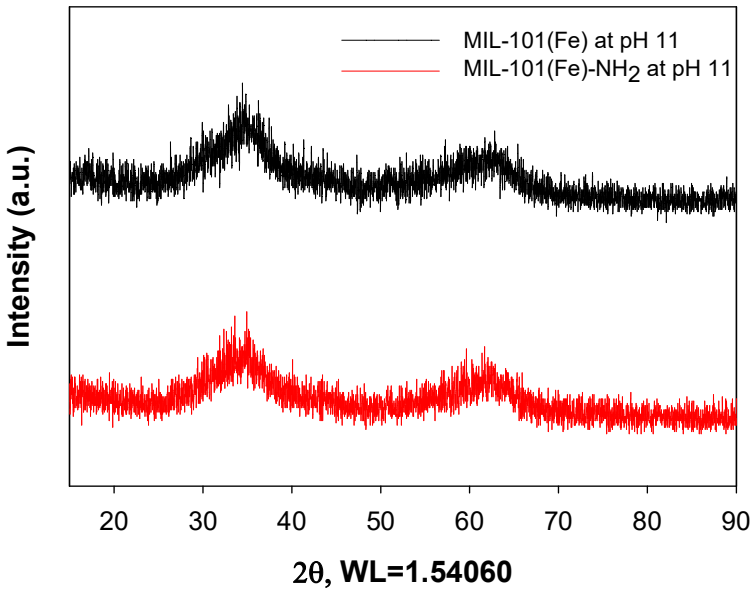

Figure. 2.2. XRD Patterns of ferrihydrite formed at pH 11 as a result of MIL-101(Fe) and MIL-101(Fe)-NH_2 destruction

Additionally, the photocatalytic degradation pathway was observed. 4-chlorophenol is known to be the product of clofibric acid oxidation (Chen et al., 2017). Hence, 4-chlorophenol concentration of the samples were measured as well. 4-chlorophenol could also be measured by the same settings of HPLC-UV used for clofibric acid measurement. The chromatography peaks of 4-chlorophenol and clofibric acid showed up at different time period. Therefore, no additional technique was involved in the 4-chlorophenol concentration measurement. Only an additional calibration function of 4-chlorophenol along with clofibric acid was applied.

2.5.2 Photocatalytic characteristics of Fe-based MOFs

To analyze the photocatalytic characteristics of MIL-101(Fe) and MIL-101(Fe)-NH_2, UV-Vis spectroscopy and X-Ray Photoelectron Spectroscopy (XPS) was used. For the bandgap energy measurement, UV-Vis spectroscopy of MIL-101(Fe) and MIL-101(Fe)-NH_2 was obtained by using (P330-30, Implen, Germany). MIL-101(Fe) and MIL-101(Fe)-NH_2 were dispersed in distilled water as a concentration of 0.1 mg/L. 4 ml of the mixture was placed in a quartz cell. Then, the absorbance of the samples in between the wavelength 300 to 700 nm were measured. For the valence band energy analysis, the XPS patterns of MIL-101(Fe) and MIL-101(Fe)-NH_2 were collected. The valence band region (-2 to 15 eV) of the XPS data was used to calculate the valence band energy.

2.5.3 Analysis of reactive oxygen species

Electron paramagnetic resonance (EPR) spectroscopy (JES-X310, Jeol, USA) was used to directly detect the presence of reactive oxygen species (ROS) in the solution. As for the radical trapper, 5,5-Dimethyl-1-pyrroline N-oxide (DMPO) was selected because DMPO was known to trap hydroxyl radical (•OH). 20 ml of distilled water was placed in the 50 ml beaker. DMPO was added to reach the concentration of 10 mM. Finally, 6 mg of MIL-101(Fe) or MIL-101(Fe)-NH_2 was added to the solution. After turning on the xenon lamp, samples were collected to measure EPR signal at the time intervals of 0, 15, 30 minutes.

3. Results and Discussion

3.1 Physiochemical properties of Fe-based MOFs

3.1.1 Physical characteristics of Fe-based MOFs

Two kinds of Fe-based MOFs, MIL-101(Fe) and MIL-101-(Fe)-NH_2 were synthesized and was investigated. FE-SEM results (Figure 3.1) indicate that MIL-101(Fe) and MIL-101(Fe)-NH_2 both possessed octahedral shapes as previously reported (Barbosa et al., 2017; Dong et al., 2020; L. He et al., 2019).

The textural properties of MIL-101(Fe) and MIL-101(Fe)-NH_2 (Table 3.1) indicated that both Fe=based MOFs have large surface areas and pore volume required for sorption of clofibric acid. Specifically, BET surface area and total pore volume calculated from the N_2 adsorption data were 1006 m^2/g and 0.545 cm^3/g for MIL-101(Fe) and 848 m^2/g and 0.412 cm^3/g for MIL-101(Fe)-NH_2, respectively. Particle diameter distribution (Fig. 3.2) was obtained from the DLS results. The mode of the distribution was selected as the representative particle size for each Fe-based MOFs. The particle diameter of MIL-101(Fe) was 568.8 nm, whereas that of MIL-101(Fe)-NH_2 was 890.5 nm. The particle size of MIL-101(Fe)-NH_2 was slightly bigger than that of MIL-101(Fe) which could be the reason of a decreased BET surface area of MIL-101(Fe)-NH_2.

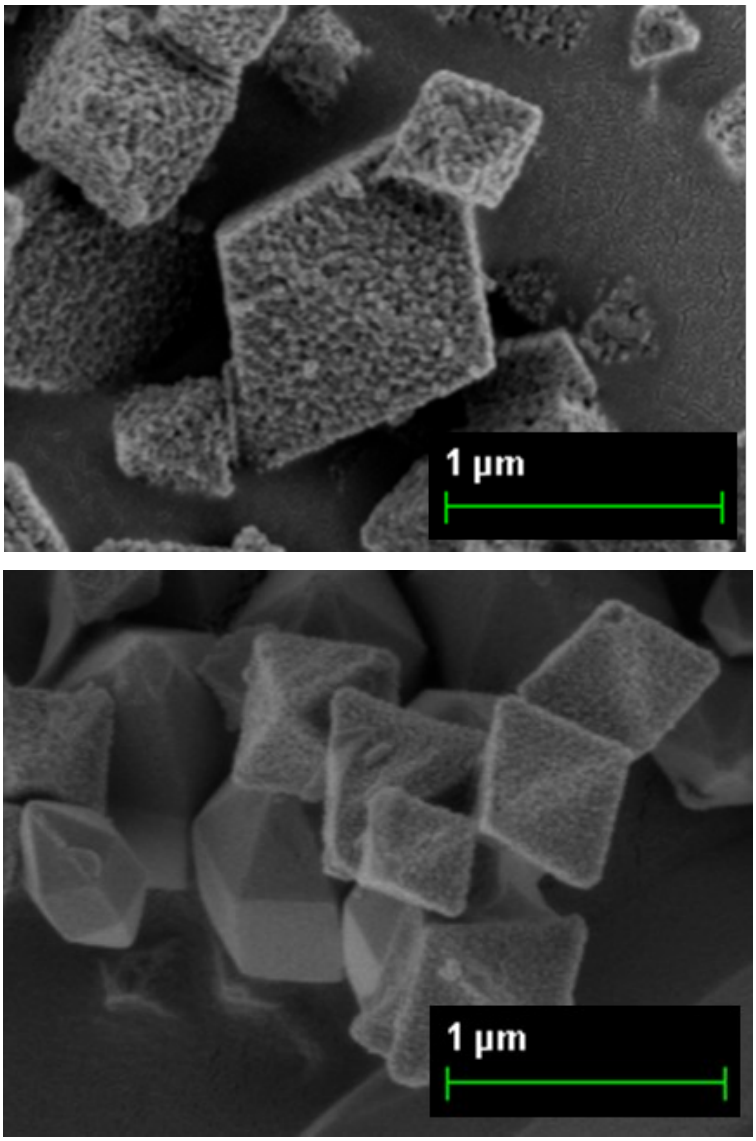

Figure. 3.1. FE-SEM results of MIL-101(Fe) (top) and MIL-101(Fe)-NH_2 (bottom)

Table 3.2. Textural properties of MIL-101(Fe) and MIL-101(Fe)-NH_2

Samples	BET surface area (m^2/g)	Total pore volume (cm^3/g)	Particle diameter [mode] (nm)
MIL-101(Fe)	1006	0.545	568.8
MIL-101(Fe)-NH_2	848	0.412	890.5

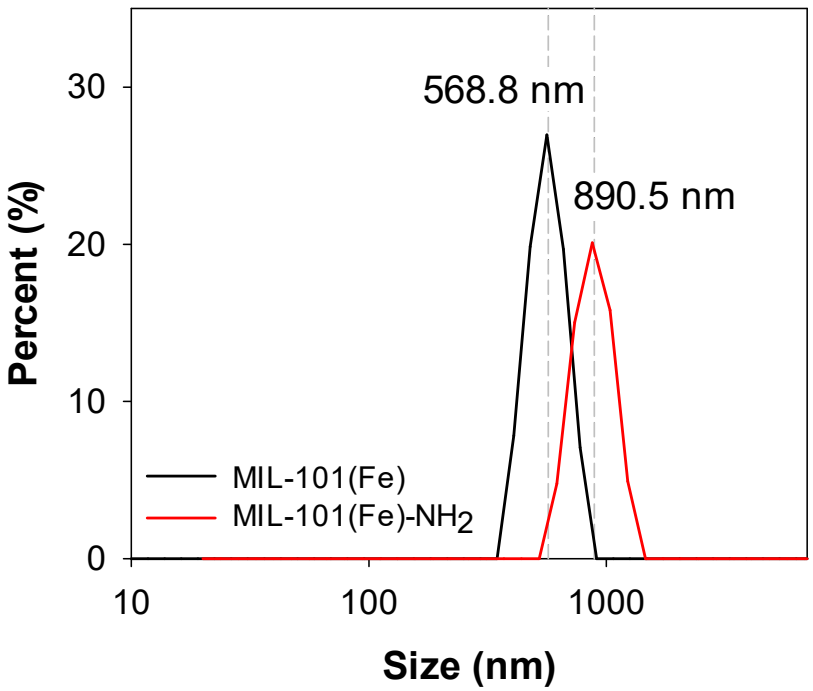

Figure. 3.2. Particle Size distribution of MIL-101(Fe) and MIL-101(Fe)-NH_2

Powder X-Ray pattern of MIL-101(Fe) and MIL-101(Fe)-NH_2 are shown in Figure. 3.3. The patterns of MIL-101(Fe) and MIL-101(Fe)-NH_2 were compared with the simulated pattern of MIL-101(Cr). The pattern of MIL-101(Cr) was simulated from the ideal crystalline data using the CIF file of MIL-101(Cr). MIL-101(Cr) is formed with the same organic ligand that of MIL-101(Fe) resulting in the similar crystalline structure that of MIL-101(Fe). Therefore, whether the main diffraction peaks of MIL-101(Fe) and MIL-101(Fe)-NH_2 follow the characteristic peaks of simulated MIL-101(Cr) is important in determining the right synthesis of two Fe-based MOFs. In result, both MIL-101(Fe) and MIL-101(Fe)-NH_2 showed clear intensity peaks with flat background. Also, the characteristic peaks of MIL-101(Cr) at 2θ = 5.16, 8.44, 9.06, 10.34, and 16.53 showed up in the peaks of MIL-101(Fe) and MIL-101(Fe)-NH_2 indicating the successful fabrication of two Fe-based MOFs.

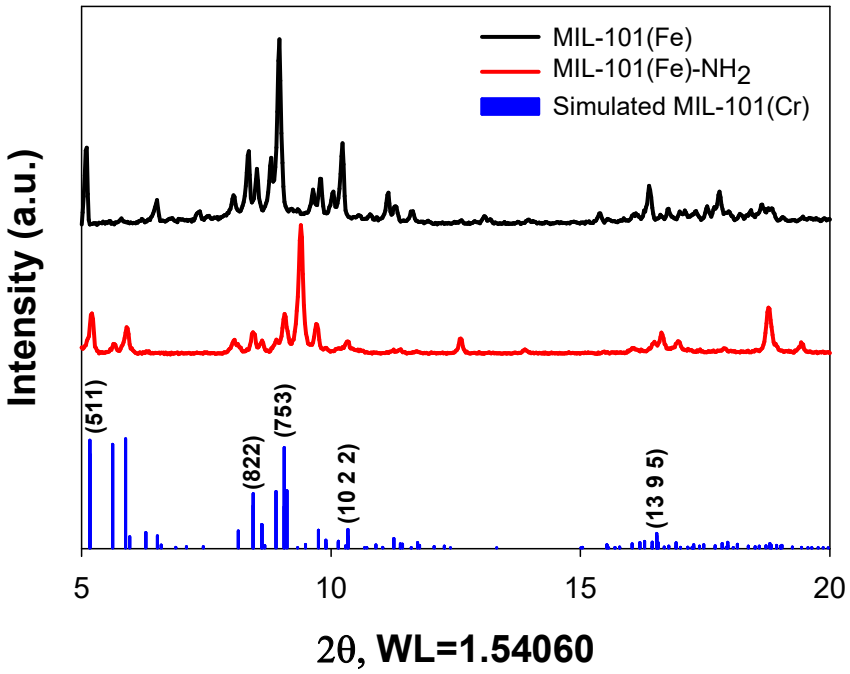

Figure. 3.3. XRD patterns of MIL-101(Fe) and MIL-101(Fe)-NH_2 compared with the simulated MIL-101(Cr) pattern

3.1.2. Chemical characteristics of Fe-based MOFs

From the FT-IR results (Figure 3.4), further molecular groups and functional groups on the surface of two Fe-based MOFs were investigated. MIL-101(Fe) and MIL-101(Fe)-NH_2 showed same peaks at the 3000-3200 cm^{-1} region, 1300-1700 cm^{-1} region, sharp peaks at 1386 cm^{-1}, and 745 cm^{-1}. These peaks indicate the O-H stretching, carboxylic group vibrations, aromatic C-C bond and Fe-O stretch respectively. The O-H vibration, carboxylic group vibrations, and the aromatic C-C bond indicate the presence of the organic ligands, BDC and 2ATA. Both ligands have the aromatic ring with two carboxylic groups attached to the ring. The Fe-O stretch is the result of the coordination bond between iron and the carboxylic group of the organic ligands. Two oxygens of the carboxylic group form coordination bonds with one iron atom and the other two oxygen atoms from the opposite carboxylic group of the same organic ligand form coordination bonds with another iron atom. Additionally, MIL-101(Fe)-NH_2 had additional peaks at 3335 cm^{-1}, and 1253 cm^{-1}. These peaks represent the primary amine group, and aromatic C-N bond, respectively. This is the result of the additional amine group attached to the amine ring in 2ATA. Hence, from FT-IR, the fabrication of MIL-101(Fe) and MIL-101(Fe)-NH_2 was once more proved to be successful and the chemical characteristics of two Fe-based MOFs was analyzed.

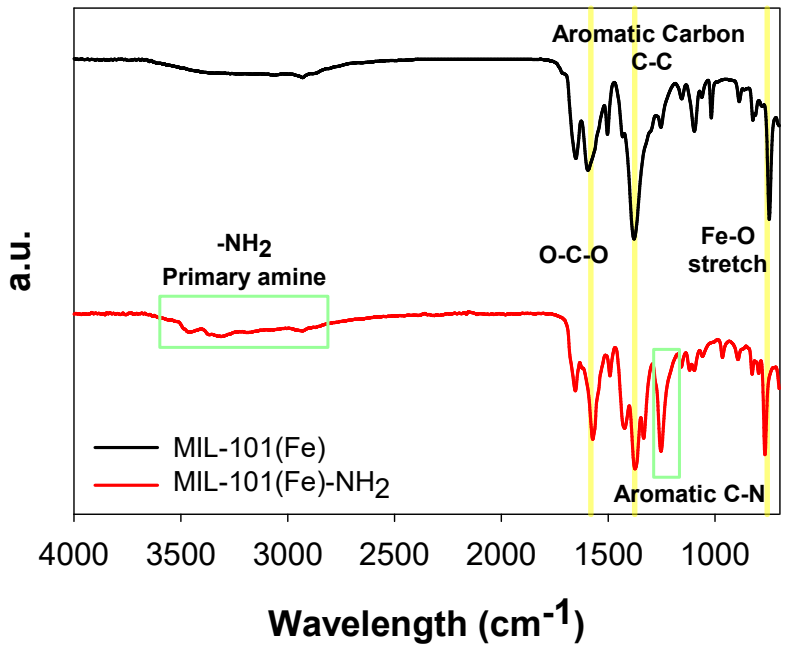

Figure. 3.4. FT-IR of MIL-101(Fe) and MIL-101(Fe)-NH_2

3.2 Sorption of clofibric acid using Fe-based MOFs

3.2.1. Sorption isotherm of clofibric acid with Fe-based MOFs

Sorption of clofibric acid using MIL-101(Fe) and MIL-101(Fe)-NH_2 was conducted at different initial concentrations of clofibric acid (C_0 = 25, 50, 100, 150 mg/L). Sorption equilibrium was reached after 30 minutes for all initial concentrations and for both Fe-based MOFs. After two hours, the removal rate of clofibric acid using MIL-101(Fe) was 57, 41, 28, 24% and that of using MIL-101(Fe)-NH_2 was 80, 56, 28, 18% at initial concentration settings of 25, 50, 100, 150 mg/L, respectively. These removal rates were reached when the amount of Fe-based MOFs were used at the concentration of 0.1 g/L respective to the solution.

The sorption isotherms of MIL-101(Fe) and MIL-101(Fe)-NH_2 were fitted using Langmuir isotherm and Freundlich isotherm (Figure 3.5). The Langmuir isotherm assumes that the sorbate is sorbed to the sorbent in a single layer due to the stronger interaction between the sorbate and sorbent compared to the interaction between sorbates. The equation for the Langmuir isotherm is as followed in equation 3.1. The term q_e is the amount of clofibric acid sorbed on to the Fe-based MOFs, Q^0 is the maximum amount of clofibric acid sorbed on to the Fe-based MOFs, C_e is the concentration of clofibric acid at the sorption equilibrium, and K_b is the Langmuir constant with the unit of L/mg. Compared to Langmuir isotherm, Freundlich isotherm assumes that the interaction between sorbates is stronger that the interaction between the sorbate and the sorbent. Therefore, it assumes that the

sorption occurs in multi-layer form. The equation for the Freundlich isotherm is as followed in the equation 3.2. K_F represents the Freundlich constant.

$$q_e = Q^0 \frac{(K_b C_e)}{1 + K_b C_e} \quad \text{(eq. 3.1)}$$

$$q_e = K_F C_e^{1/n} \quad \text{(eq. 3.2)}$$

Consequently, the fitting results for two isotherm models are shown in Table 3.2. The isotherm of MIL-101(Fe) was fitted better by Freundlich isotherm whereas the isotherm of MIL-101(Fe)-NH_2 was fitted better by Langmuir isotherm. Therefore, from the sorption isotherm results, it can be assumed that the sorption of clofibric acid on to MIL-101(Fe) occurs in multi-layers, whereas the sorption on to MIL-101(Fe)-NH_2 occurs in a single layer form. As the sorption occurs in a single-layer form, once the sorption capacity is reached, no additional clofibric acid molecules can be sorbed. The sorption capacity can be calculated by the fitting of Langmuir isotherm. Hence, the sorption capacity for MIL-101(Fe)-NH_2 was 290.03 mg-clofibric acid/g-MOF. Compared to MIL-101(Fe), MIL-101(Fe) could sorb additional clofibric acid molecules and the amount of the sorbed clofibric acid molecules depended on the concentration of clofibric acid in the solution. As the aqueous concentration of clofibric acid increased, the amount of sorbed clofibric acid also increased which was determined by Freundlich isotherm.

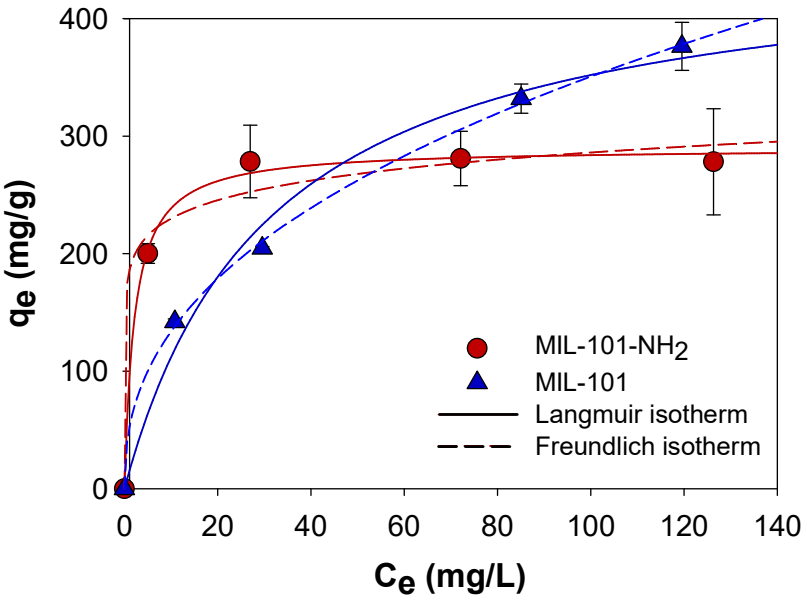

Figure. 3.5. Sorption isotherm of clofibric acid on MIL-101(Fe) and MIL-101(Fe)-NH_2

Table 3.2. Sorption isotherm models and parameters of clofibric acid on MIL-101(Fe) and MIL-101(Fe)-NH_2

Langmuir isotherm $q_e = Q^0 \frac{(K_b C_e)}{1+K_b C_e}$			
Sorbents	K_b (L/mg)	Q_0 (mg/g)	R^2
MIL-101(Fe)-NH_2	0.465	290.03	0.997
MIL-101(Fe)	0.032	461.85	0.988

Freundlich isotherm $q_e = K_F C_e^{1/n}$			
Sorbents	K_F	1/n (n)	R^2
MIL-101(Fe)-NH_2	184.86	0.095	0.975
MIL-101(Fe)	51.05	0.419	0.999

3.2.2. Sorption kinetics of clofibric acid with Fe-based MOFs

Sorption kinetics of clofibric acid using MIL-101(Fe) and MIL-101(Fe)-NH_2 was also determined (Figure 3.6). The sorption kinetics of clofibric acid with both Fe-based MOFs at all initial concentration conditions followed the pseudo-second order kinetic. The pseudo-second order kinetic sorption model can be described with the equation 3.3. The parameter q_e represents the amount of sorbed clofibric acid onto Fe-based MOFs, and the parameter k_2 represents the pseudo-second order kinetic constant, both of which can be calculated by fitting the model. By drawing a graph having time at the x-axis and amount of clofibric acid divided by time at the y-axis, the graph takes a linear form having $1/q_e$ as the slope and $1/k_2q_e^2$ as the y-axis intercept.

$$\frac{t}{q_t} = \left[\frac{1}{k_2 q_e^2}\right] + \frac{t}{q_e} \qquad \text{(eq. 3.3)}$$

The parameters of the pseudo-second kinetic model for each Fe-based MOFs can be found in Table 3.3. The maximum amount of clofibric acid (q_e) was calculated to be 143, 208, 333, and 385 mg/g for MIL-101(Fe) at initial concentrations of 25, 50, 100, and 150 mg/L, respectively, whereas that for MIL-101(Fe)-NH_2 were 200, 233, 286, and 286 mg/g. At the initial concentration smaller that 50 mg/L the maximum sorbed amount of clofibric acid was larger for MIL-101(Fe)-NH_2 than MIL-101(Fe). In comparison, at the initial concentration conditions larger that 100 mg/L, the maximum sorbed amount of clofibric acid was larger for

MIL-101(Fe) than MIL-101(Fe)-NH_2. This is consistent with the sorption isotherm results because it indicates that the sorption capacity of MIL-101(Fe)-NH_2 is limited compared to MIL-101(Fe) which is more influenced by the aqueous concentration of clofibric acid. Also, this is consistent with the BET surface area data since the surface area for MIL-101(Fe) was larger than MIL-101(Fe)-NH_2.

By comparing the pseudo-second kinetic constant of two Fe-based MOFs, constants at all initial concentration conditions were larger for MIL-101(Fe)-NH_2 than MIL-101(Fe) (Table 3.3). At the initial concentration conditions of 25, 50, 100, 150 mg/L, the pseudo-second order kinetic constants for MIL-101(Fe) were 0.163, 0.115, 0.045, and 0.087, respectively, and that for MIL-101(Fe)-NH_2 were 0.751, 0.192, 0.133, 0.298. This indicates that the sorption interaction of MIL-101(Fe)-NH_2 with clofibric acid was stronger than the interaction of MIL-101(Fe). The difference between MIL-101(Fe) and MIL-101(Fe)-NH_2 is the presence of amine functional group. Hence, it can be inferred that the interaction between clofibric acid molecules and MIL-101(Fe)-NH_2 is mostly caused by the interaction between clofibric acid and the amine group.

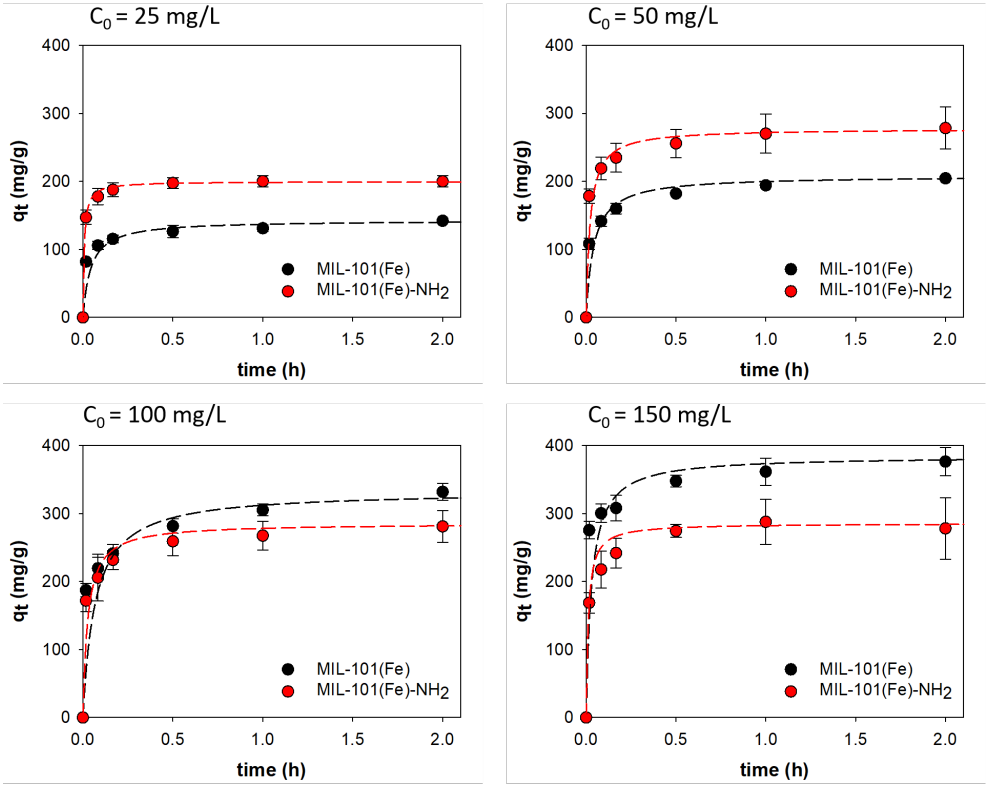

Figure. 3.6. Sorption kinetics of clofibric acid on MIL-101(Fe) and MIL-101(Fe)-NH_2 at different initial concentrations

Table 3.3. Pseudo-seconder kinetic constants (k_2) of MIL-101(Fe) and MIL-101(Fe)-NH_2 at different initial concentrations

Pseudo-second order kinetic constant (k_2) (g/mg-h)		
Initial CFA conc. (mg/L)	MIL-101(Fe)	MIL-101(Fe)-NH_2
25	0.163	0.751
50	0.115	0.192
100	0.045	0.133
150	0.087	0.298

3.2.3 Sorption thermodynamics of clofibric acid with Fe-based MOFs

In order to further interpret the sorption mechanism between clofibric acid and Fe-based MOFs, thermodynamic parameters were obtained. As the presence of the amine group differentiates the sorption mechanism between MIL-101 and MIL-101(Fe)-NH_2, it can be inferred that the thermodynamic of the sorption will also show difference and can help explain the specific sorption mechanisms between clofibric acid molecules and Fe-based MOFs.

Thermodynamic parameters can be obtained from the sorption isotherm data at different temperatures. The sorption isotherm of clofibric acid with two Fe-based MOFs is shown in Figure 3.7. Sorption isotherms were all fitted using Langmuir isotherm which the constants are written in Table 3.4.

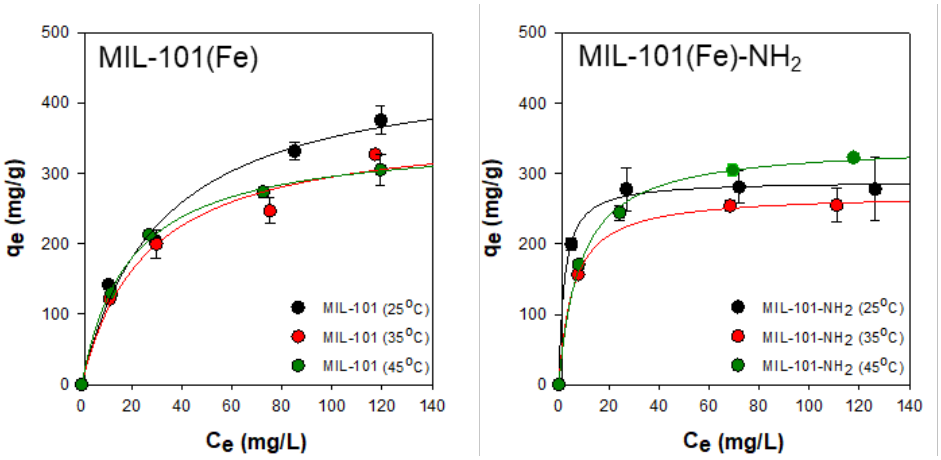

Figure. 3.7. Sorption isotherm of clofibric acid on MIL-101(Fe) and MIL-101(Fe)-NH_2 at various temperature conditions

Table 3.4. Langmuir constants (K_b) of MIL-101(Fe) and MIL-101(Fe)-NH_2 at various temperatures

Langmuir constant (K_b) (L/mol)		
Temperature (K)	MIL-101(Fe)	MIL-101(Fe)-NH_2
298	6869	99853
308	8307	38529
318	11183	25178

Using the Langmuir constants, van' t Hoff plot (Figure 3.8) could be drawn according to the van' t Hoff equation (eq. 3.4) With $\ln(K_b)$ at the y-axis and 1/T at the x-axis, a line can be drawn using the sorption isotherm data obtained at different temperatures. The slope of the linear function is -(ΔH/R) and the y-axis intercept is (ΔS/R) according to the van't Hoff equation. R is the gas constant, 8.314 J/mol•K. Hence, the enthalpy change (ΔH) and the entropy change (ΔS) can be calculated from the plot.

$$\ln K_b = \frac{\Delta S}{R} - \frac{\Delta H}{RT} \qquad \text{(eq. 3.4)}$$

Gibb' s free energy can be also calculated using the Langmuir constant at different temperatures. (equation 3.5)

$$\Delta G = -RT \ln K_b \qquad \text{(eq. 3.5)}$$

The calculated thermodynamic parameters of the sorption of clofibric acid onto two Fe-based MOFs are shown in Table 3.4. Gibb's free energy difference of the sorption were negative at all temperatures and for both Fe-based MOFs indicating that the sorption reaction is a spontaneous reaction. Specifically, the absolute value of the Gibb's free energy difference got bigger as temperature increased for MIL-101(Fe), whereas it got smaller for MIL-101(Fe)-NH_2.

Furthermore, the enthalpy change (ΔH) and the entropy change (ΔS) were both positive for MIL-101(Fe) and both negative for MIL-101(Fe)-NH_2. This indicates that the sorption of clofibric acid onto MIL-101(Fe) is an endothermic reaction and the sorption onto MIL-101(Fe)-NH_2 is an exothermic reaction. If the enthalpy change is negative for the sorption phenomena, it infers that the sorption occurs as the form of adsorption that is, the sorption of the clofibric acid molecules mainly occurs on the surface of the sorbent. Hence, as the enthalpy change for the sorption onto MIL-101(Fe)-NH_2 is negative, it can be concluded that the sorption happens on the surface of MIL-101(Fe)-NH_2.

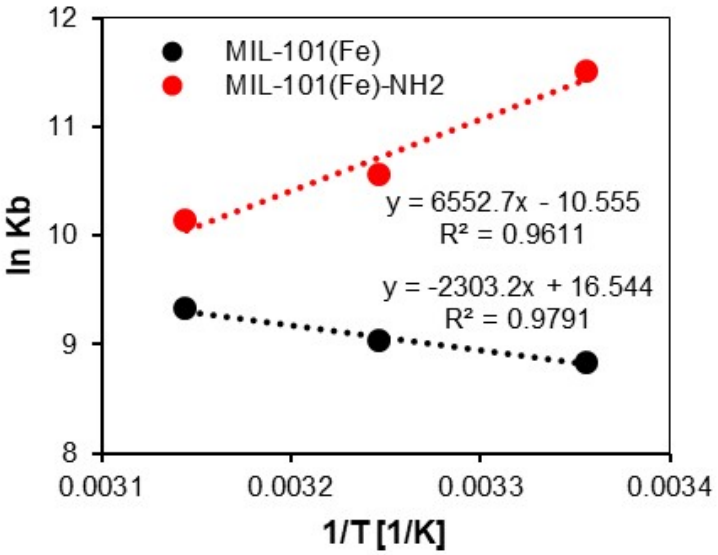

Figure. 3.8. van't Hoff plot of the sorption of clofibric acid with MIL-101(Fe) and MIL-101(Fe)-NH_2

Table 3.5. Thermodynamic parameters of the sorption of clofibric acid with MIL-101(Fe) and MIL-101(Fe)-NH_2

	MIL-101(Fe)			MIL-101(Fe)-NH_2		
Temperature (K)	ΔG (kJ/mol)	ΔH (kJ/mol)	ΔS (J/mol·K)	ΔG (kJ/mol)	ΔH (kJ/mol)	ΔS (J/mol·K)
298	−21.89	19.15	137.5	−28.52	−54.48	−87.8
308	−23.11			−27.04		
318	−24.65			−26.79		

Combining the results of the sorption isotherms and kinetics, it can be inferred that clofibric acid molecules are attracted to the amine group on the surface of MIL-101(Fe)-NH_2 and the already sorbed clofibric acid molecules hinder other molecules from entering the pores of MIL-101(Fe)-NH_2. Since the sorption of clofibric acid only occurs on the surface amine groups, only a single layer of clofibric acid can be sorbed to the sorbent. This can explain why the sorption of MIL-101(Fe)-NH_2 followed Langmuir isotherm having a limited maximum sorption capacity. From the molecular structure of clofibric acid, it can be suggested that the carboxylic group of the molecule forms strong acid-base interaction with the amine group of MIL-101(Fe)-NH_2. This strong interaction may be the reason for the faster sorption kinetic compared to MIL-101(Fe).

On the contrary, clofibric acid sorption with MIL-101(Fe) may occur both on the surface and the pores through various sorption mechanisms. The possible interaction between clofibric acid molecules and MIL-101(Fe) may include $\pi-\pi$ interaction between the aromatic rings of clofibric acid and the organic ligand, and coordination of clofibric acid with unsaturated sites of center iron ion. Especially, as $\pi-\pi$ interaction can lead to $\pi-\pi$ stacking, this may explain why the sorption of clofibric acid with MIL-101(Fe) did not show a limited sorption capacity and showed increasing sorption capacity depending on the aqueous concentration of clofibric acid.

3.2.4 Sorption mechanisms of clofibric acid with Fe-based MOFs depending on pH

These mechanisms can be further explained by the FT-IR spectroscopy results obtained after the sorption of clofibric acid at various pH range (Figure 3.9). The FT-IR results after sorption was compared to the FT-IR result obtained after soaking MIL-101(Fe) and MIL-101(Fe)-NH_2 in DI at pH 4. The region for surface functional groups, carboxylic group and amine group was compared among FT-IR results. For MIL-101(Fe), there was only a little difference between the peaks of MIL-101(Fe) soaked in DI and that of obtained after sorption at pH 2, 4, and 6. The FT-IR result obtained after sorption at pH 8 showed unclear peaks which was due to the collapse of the crystal structure of MIL-101(Fe) forming ferrihydrite. Compared to MIL-101(Fe), FT-IR results of MIL-101(Fe)-NH_2 showed decreased peaks in the region of N-H stretch and aromatic C-N after sorption at all pH conditions. This indicates that the sorbed clofifibric acid molecules sobbed on the surface, especially at amine groups, hindering the detection of amine groups. Furthermore, comparing between the FT-IR results at various pH conditions, only the N-H stretch region showed difference and coincided at other regions. This indicates that the sorption of clofibric acid onto MIL-101(Fe)-NH_2 was altered by pH due to pH-dependent form of the amine group.

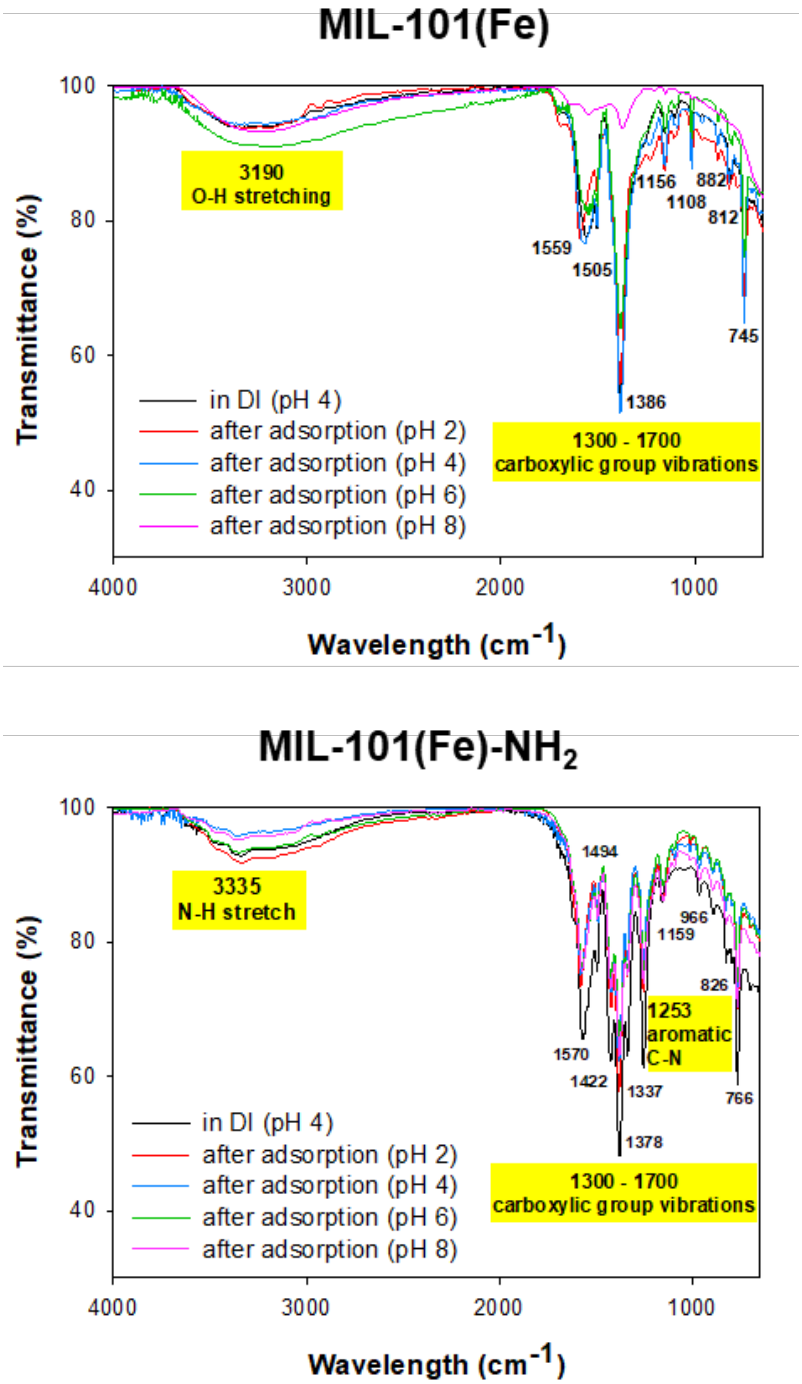

Figure. 3.9. FT-IR of MIL-101(Fe) (top) and MIL-101(Fe)-NH_2 (bottom) before and after the adsorption of clofibric acid at various pH conditions

The pH dependent sorption mechanism can be further expounded by the result of the sorption of clofibric acid at various pH conditions (Figure 3.10). The highest sorption capacity was achieved at pH 4 for both Fe-based MOFs. At lower pH, the sorption capacity slightly decreased and at higher pH, the sorption capacity drastically decreased. Especially, MIL-101(Fe) and MIL-101(Fe)-NH_2 were unable to sorb any clofibric acid at above pH 7 and pH 9, respectively. This was due to the destruction of the crystallinity of Fe-based MOFs at basic conditions from the breakage of coordination bonds between center iron ion and organic ligands.

Since clofibric acid and organic ligand both are affected by pH, the sorption of clofibric acid is greatly affected by pH. The pKa value of clofibric acid is 3.18 whereas the pKa value of the aromatic amine group in the 2ATA organic ligand is 4.5. This indicates that the carboxylic group of the clofibric acid will be neutrally charged at pH below 3.18 and negatively charged at pH above 3.18 due to the detachment of the hydrogen ion. On the other hand, the amine group attached to the organic ligand will be positively charged at pH below 4.5 and neutrally charged at pH higher than 4.5. Hence, in between pH 3.18 to 4.5, clofibric acid and the amine group is oppositely charged leading to an electrostatic interaction among them. Due to this additional interaction mechanism, sorption of clofibric acid on MIL-101(Fe)-NH_2 increases compared to other pH conditions.

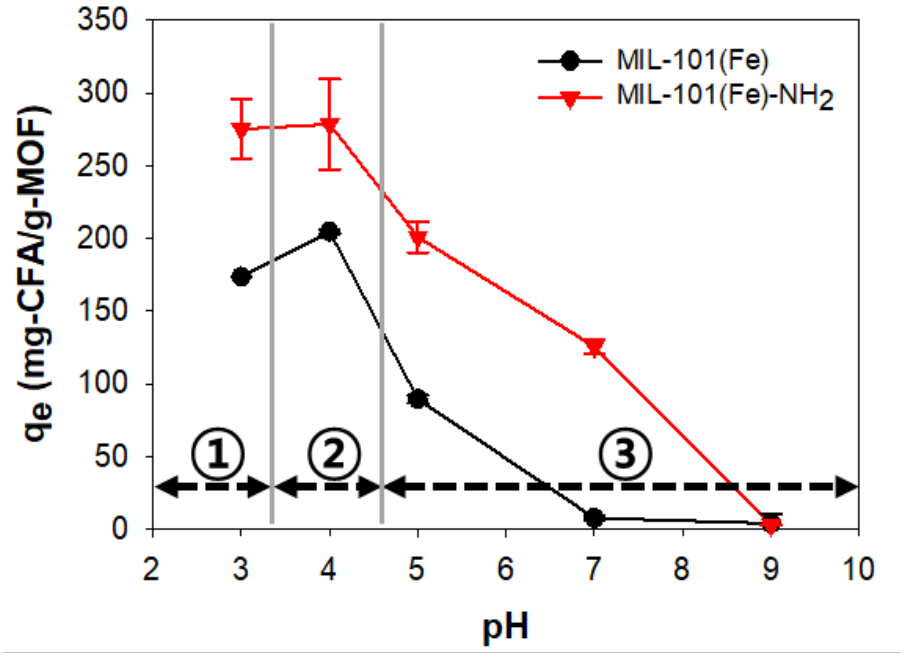

Figure. 3.10. Sorption of clofibric acid with MIL-101(Fe) and MIL-101(Fe)-NH_2 at various pH conditions

3.3 Photocatalytic degradation of clofibric acid using Fe-based MOFs

3.3.1 Removal of clofibric acid through photocatalytic degradation using Fe-based MOFs

With xenon lamp equipped with UV-cutoff filter as the light source, the removal of clofibric acid was observed for 24 hours (Figure 3.11). As described, the aqueous concentration and the total concentration including the portion sorbed on to Fe-based MOFs were both measured. After 30 minutes, time required to reach the sorption equilibrium, the aqueous concentration of clofibric acid decreased to 23% for MIL-101(Fe) and 4% of the initial concentration, 50 mg/L. After the irradiation of xenon lamp for 24 hours, the aqueous clofibric acid concentration decreased 98.8% for MIL-101(Fe) and 99.4% for MIL-101(Fe)-NH_2 compared to the initial concentration. However, significant amount of clofibric acid was sorbed onto Fe-based MOFs. After 24 hours, the total clofibric acid concentration decreased to 49.7% for MIL-101(Fe) and 5.5% for MIL-101(Fe)-NH_2 compared to the initial concentration. This indicated that only about half of the total clofibric acid molecules were photocatalytically degraded from the photocatalytic activity of MIL-101(Fe) and very little photocatalytic behavior was observed for MIL-101(Fe)-NH_2.

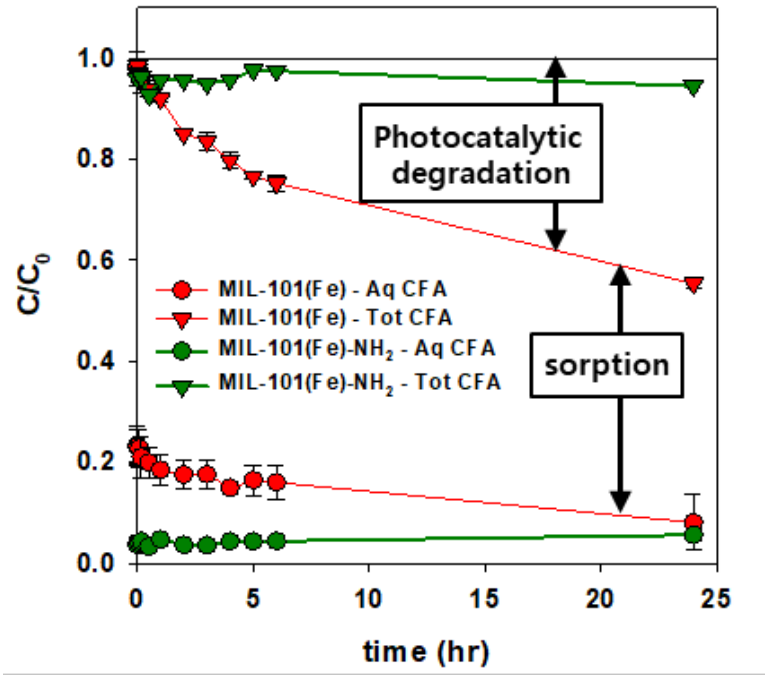

Figure. 3.11. Photocatalytic degradation of clofibric acid using MIL-101(Fe) and MIL-101(Fe)-NH_2

3.3.2 Kinetic of photocatalytic degradation of clofibric acid using MIL-101(Fe)

Since the significant amount of photocatalytic degradation of clofibric acid was only observed using MIL-101(Fe), the degradation kinetic of clofibric acid was described only for MIL-101(Fe). Since the total concentration of clofibric acid reflects the photocatalytically degraded amount of clofibric acid, only the total concentration was used to describe the degradation kinetic. Three types of kinetic models, zero-order, pseudo-first-order, and pseudo-second-order reaction models, were used to explain the photocatalytic degradation kinetic (Figure 3.12). Kinetic constants and r-square for the model were listed in Table 3.6. As a result, pseudo-second-order reaction model most successfully described the photocatalytic degradation kinetic of clofibric acid. Pseudo-second-order reaction model follows the form of equation 3.6. $k_{photo,2}$ is the pseudo-second-order kinetic constant with the unit of $mg^{-1}\cdot L\cdot h^{-1}$. The pseudo-second-order kinetic constant for the photocatlytic degradation of clofibric acid using MIL-101(Fe) was 8.74×10^{-4} $mg^{-1}\cdot L\cdot h^{-1}$.

$$C = \frac{C_0}{1 + k_{photo,2} t C_0} \qquad \text{(eq. 3.6)}$$

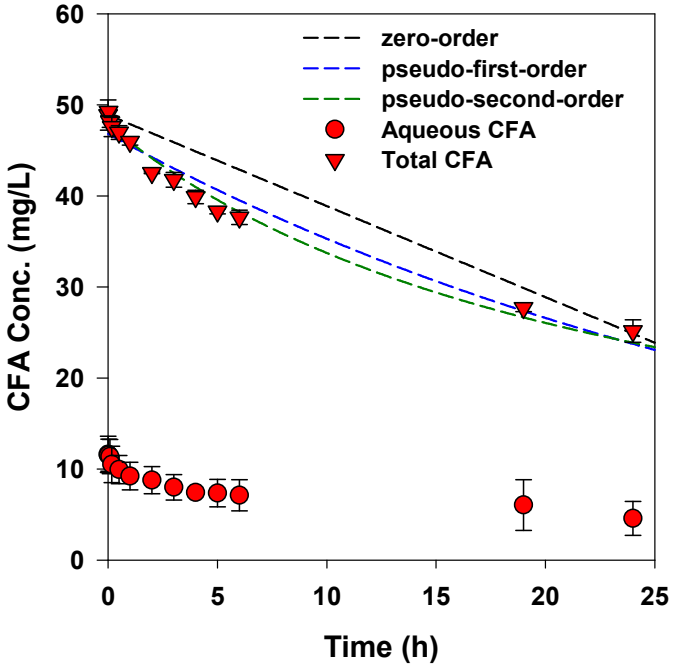

Figure. 3.12. Photocatalytic degradation kinetic of clofibric acid using MIL-101(Fe)

Table 3.6. Photocatalytic degradation kinetic models and kinetic constants of clofiric acid using MIL-101(Fe)

Kinetic model	Zero-order reaction $C = C_0 - k_{photo,0}t$	Pseudo-first-order reaction $C = C_0 \exp(-k_{photo,1}t)$	Pseudo-second-order reaction $C = \frac{C_0}{1 + k_{photo,2}tC_0}$
Kinetic constant	$k_{photo,0}$ ($mg \cdot L^{-1} \cdot h^{-1}$)	$k_{photo,1}$ (h^{-1})	$k_{photo,2}$ ($mg^{-1} \cdot L \cdot h^{-1}$)
	1.00	2.83×10^{-2}	8.74×10^{-4}
R^2	0.82	0.964	0.983

3.3.3 Pathway of photocatalytic degradation of clofibric acid

The oxidation pathway of clofibric acid was expounded by past studies. (Chen et al., 2017) Before mineralization, 4-chlorophenol was found to be the intermediate of the oxidation of chlorophenol. Hence, in this study, the production of 4-chlorophenol was also observed.

The concentration of 4-chlorophenol was also measured in two different ways accounting for the aqueous portion and the total amount of the 4-chlorophenol. As a result, when MIL-101(Fe) was used as a photocatalyst, production of 4-chlorophenol was observed. Converting the units into mmol/L, 0.12 mM of clofibric acid was degraded and 0.13 mM of 4-chlorophenol was produced after 24 hours. This in result indicates that the decrease of clofibric acid observed in Figure 3.11 could be expounded by the photocatalytic oxidation of clofibric acid to form 4-chlorophenol as intermediates. In comparison, only a small amount of 4-chlorophenol was produces when MIL-101(Fe)-NH_2 was utilized as a photocatalyst. This was an expected result as the total concentration of clofibric acid did not decrease in Figure 3.11. Therefore, once again, MIL-101(Fe)-NH_2 proved to possess limited photocatalytic ability. Additionally, only 4-chlorophenol was used as the target substance for the sorption and photocatalytic degradation using MIL-101(Fe) and MIL-101(Fe)-NH_2. The results indicated that 4-chlorophenol did not sorb nor degrade in the process (Figure 3.14). This indicates that during the process of clofibric acid oxidation, 4-chlorophenol was the final product of the process rather than being the intermediate substance.

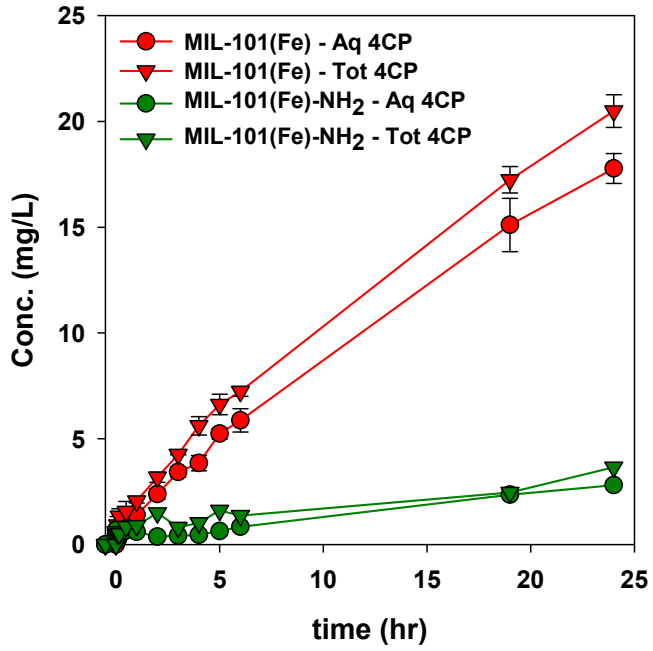

Figure. 3.13. Formation of 4-chlorophenol during photocatalytic degradation of clofibric acid using MIL-101(Fe) and MIL-101(Fe)-NH_2

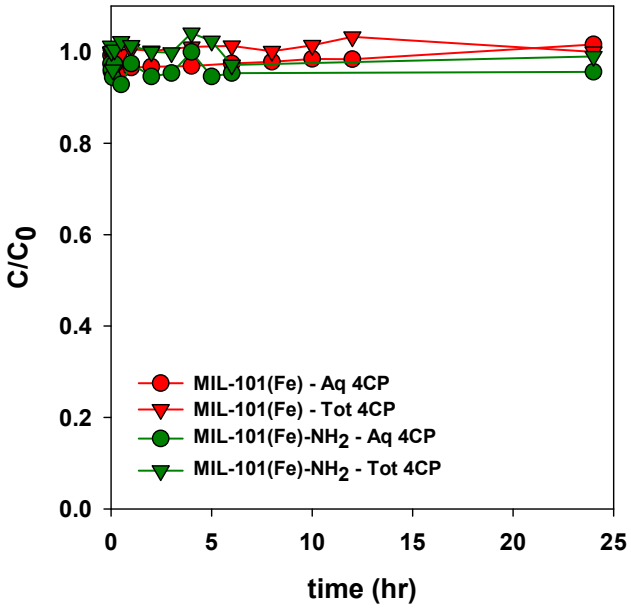

Figure. 3.14. Photocatalytic degradation of 4-chlorophenol using MIL-101(Fe) and MIL-101(Fe)-NH_2

3.3.4 Photocatalytic activity of Fe-based MOFs

3.3.4.1 Bandgap structure of Fe-based MOFs

The bandgap structure is the key characteristic that determines the photocatalytic activity of a photocatalyst. The bandgap energy is directly related to the light wavelength the photocatalyst can utilize. Based on the results of Planck's equation, the bandgap needs to be smaller than 3.26 eV in order to utilize visible light (Bedia et al., 2019).

The bandgap energy can be calculated from the Tauc method (Ramalho et al., 2021). Tauc method is a commonly used method to estimate the bandgap energy of amorphous semiconductors. It can be derived from the UV-vis spectroscopy adsorption data, The main equation of Tauc method is stated in equation 3.7 α is the absorption coefficient, h is Planck constant, ν is photon's frequency, Eg is the bandgap energy and B is a constant. The left side of the equation can be calculated from the absorption data through equation 3.8. A is the absorbance and E is the energy of the certain wavelength of light.

$$(\alpha h\nu)^2 = B(h\nu - E_g) \quad \text{(eq. 3.7)}$$

$$(\alpha h\nu)^2 = (2.303 * A * E)^2 \quad \text{(eq. 3.8)}$$

Through deriving the absorption data from UV-vis spectroscopy, Tauc graph can be drawn using the upper equations. Figure 3.15 illustrates the Tauc graph of MIL-101(Fe) and MIL-101(Fe)-NH_2. The bandgap energy is the x-axis intercept of the regression line drawn in the incrementing part of the graph. As a result, the bandgap energy of MIL-101(Fe) was 2.37 eV and that of MIL-101(Fe)-NH_2 was 1.36 eV. Both bandgap energies were small enough to utilize visible light. The amine functionalization of the Fe-based MOF reduced the bandgap. This can be explained by the similar phenomenon reported by De Vos et al., [2017], which the amine functionalized UiO-66 narrowed the bandgap energy. The reason for the decreased bandgap of amine functionalized MOF was attributed to a newly generated electron state between HOMO and LUMO because of the electron donation of the amine group towards the aromatic ring of the organic ligand. Same explanation can be the reason for the narrower bandgap of MIL-101(Fe)-NH_2 compared to MIL-101(Fe).

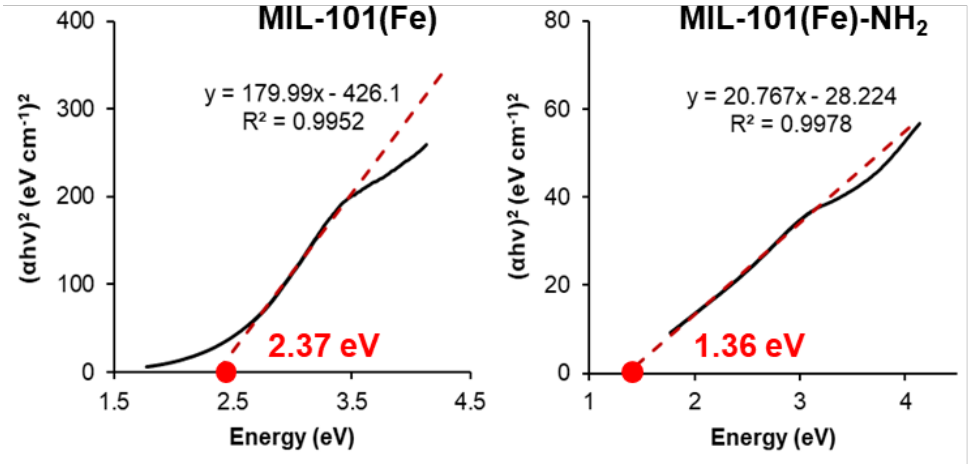

Figure. 3.15. Tauc plot of MIL-101(Fe) and MIL-101(Fe)-NH_2

The valence band energy level can be derived from the valence band region of the XPS data (Kraut et al., 1980). The valence band region is the region showing the binding energy level of −2 to 15 eV. At this region, a regression line can be drawn at the first increasing part of the XPS data. Valence band energy is the x−axis intercept of this line. The valence band region of the XPS data of MIL−101(Fe) and MIL−101(Fe)−NH_2 is shown in Figure 3.16. Regression lines were drawn for both graphs. Consequently, the valence band energy for MIL−101(Fe) and MIL−101(Fe)−NH_2 was 1.74 eV and 1.44 eV, respectively.

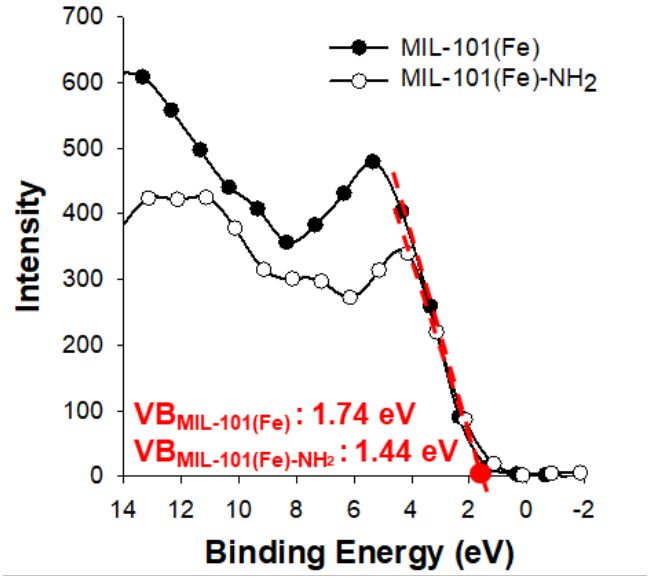

Figure. 3.16. Valence band region of XPS of MIL−101(Fe) and MIL−101(Fe)−NH_2

Conduction band energy can be calculated using the derived valence band energy and the bandgap energy. By simply subtracting the value of the bandgap energy from the valence band energy, conduction band energy can be derived. As a result, the conduction band energy for MIL-101(Fe) and MIL-101(Fe)-NH_2 was -0.63 eV and 0.08 eV, respectively. Table 3.7 sates the bandgap structure for both Fe-based MOFs.

Table 3.7, Bandgap energy levels of MIL-101(Fe) and MIL-101(Fe)-NH_2

	MIL-101(Fe)	MIL-101(Fe)-NH_2
E_{CB}	-0.63 eV	0.08 eV
E_{VB}	1.74 eV	1.44 eV
E_g	2.37 eV	1.36 eV

Based on the bandgap energy levels of MIL-101(Fe) and MIL-101(Fe)-NH_2, the photocatalytic degradation mechanism of clofibric acid was expounded. As for MIL-101(Fe), there could be three pathways for the oxidation of clofibric acid (Figure 3.17). The first pathway is the direct oxidation of clofibric acid through the hole in the valence band of MIL-101(Fe). After the electron is excited, holes in the valence band can serve as oxidants trying to obtain an extra electron near itself. Hence, it can result in the oxidation of the sorbed clofibric acid molecules. The second and third pathway starts with the production of superoxide anions. The conduction band energy of MIL-101(Fe) is lower than the redox potential needed for the reduction of oxygen to form superoxide

anion radicals. Therefore, once the electron is excited to the conduction band, it can be utilized for the reduction reaction of oxygen to for superoxide anions. Superoxide radical is a reductant rather than an oxidant. Still, superoxide radicals can react with water molecules to product hydroxyl radicals. Hydroxyl radicals are very powerful oxidants which can accelerate the oxidation of clofibric acid. As the formation of superoxide anion occurs at the surface of MIL-101(Fe), the hydroxyl radical is formed on the surface, too. Hence, the second pathway of the oxidation of clofibric acid is the direct oxidization of sorbed clofibric acid molecules by the hydroxyl radicals on the surface. The third pathway requires the diffusion of superoxide anion from the surface to be aqueous states. Once the superoxide radical is diffused, it can also be transformed into hydroxyl radicals, also in aqueous states, which can oxidize the aqueous clofibric acid molecules. Summing up, MIL-101(Fe) is capable of oxidizing both the clofibric acid in the sorbed state and the aqueous state.

In comparison, MIL-101(Fe)-NH_2 has only one oxidation pathway of clofibric acid (Figure 3.18). Because the conduction band energy of MIL-101(Fe)-NH_2 has higher energy that the redox potential of the reduction of oxygen into superoxide radical, no radicals can be produced by the photocatalytic activity of MIL-101(Fe)-NH_2. The electron in the valence band can still be excited by the absorption of light to form holes. These holes are capable of the oxidation of clofibric acid sorbed on to the surface. This is the only pathway clofibric acid can be oxidized. Hence, this may be the reason for the low photocatalytic degradation of clofibric acid when MIL-101(Fe)-NH_2 is used as a photocatalyst.

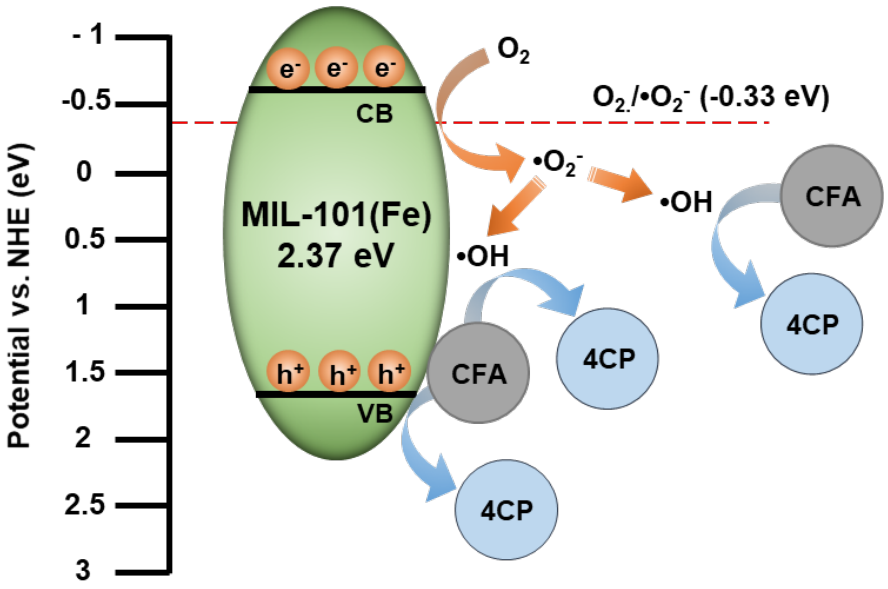

Figure. 3.17. The schematic diagram of the photocatlytic degradation of clofibric acid using MIL-101(Fe)

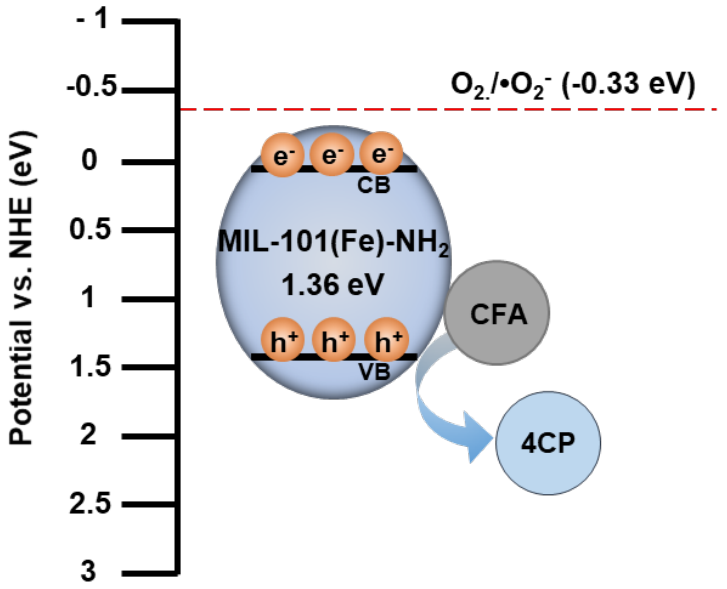

Figure. 3.18. The schematic diagram of the photocatlytic degradation of clofibric acid using MIL-101(Fe)-NH_2

3.3.4.2 Formation of reactive oxygen species from Fe-based MOFs

The formation of reactive oxygen species using MIL-101(Fe) and MIL-101(Fe)-NH_2 was analyzed using EPR (Figure 3.19). The EPR results can be interpreted by the formation of the EPS signals. The location of the peaks and their relative ratio determines the type of radical that is formed in the reactor (J. He et al., 2018).

For MIL-101(Fe), 4 clear peaks with the intensity ratio of 1:2:2:1 was observed in the EPR signal. This indicates the formation of hydroxyl radicals. Comparing the signal intensities by time, the intensity of the EPR signal increased until 30 minutes. This is in coincidence with the possible photocatalytic degradation mechanism of clofibric acid using MIL-101(Fe) because at first, superoxide anion radicals are formed and as time passes, superoxide radicals react with water molecules to form hydroxyl radicals. Therefore, the increasing concentration of hydroxyl radicals indicate that through the photocatalytic activities of MIL-101(Fe), superoxide radicals are transformed into hydroxyl radicals.

On the other hand, the EPR signal for MIL-101(Fe)-NH_2 did not show any clear signals at all time points. This is again an evidence that MIL-101(Fe)-NH_2 has the bandgap unable to create any reactive oxygen species through the excitation of electron.

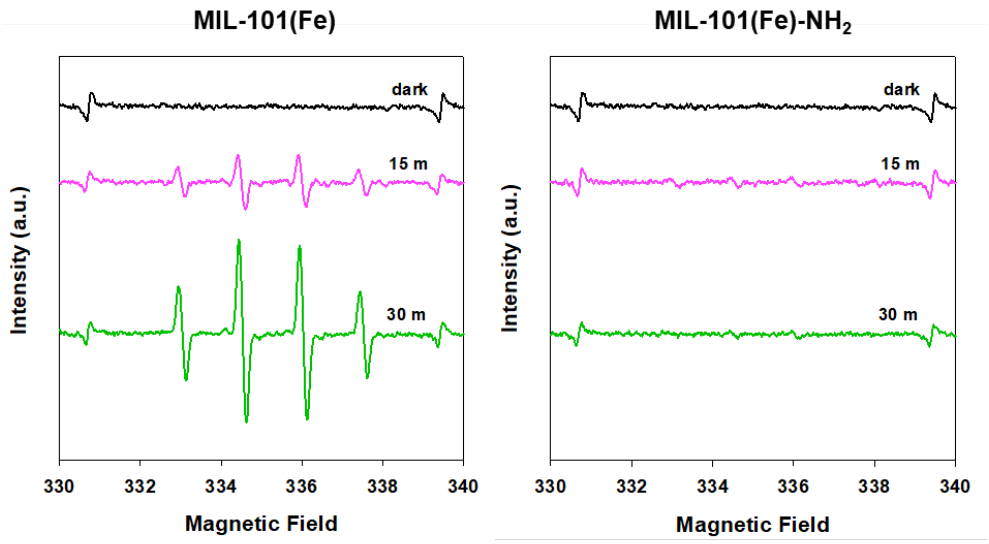

Figure. 3.19 EPR signals of MIL-101(Fe) (left) and MIL-101(Fe)-NH_2 (right) after 0, 15, and 30 minutes

4. Conclusions

MIL-101(Fe) and MIL-101(Fe)-NH_2 were synthesized and used as sorbents and photocatalysts for the removal of clofibric acid. Due to the presence of the amine functional group of MIL-101(Fe)-NH_2, sorption and photocatalytic mechanisms toward clofibric acid changed compared to MIL-101(Fe).

FE-SEM, XRD, and FT-IR data inferred that MIL-101(Fe) and MIL-101(Fe)-NH_2 had clear crystal shapes and functional groups that stemmed from organic ligands. Also, both had large BET surface areas, 1006, and 848 m^2/g, respectively, indicating enough capability to be used as sorbents.

When clofibric acid was sorbed to Fe-based MOFs, the sorbed amount was larger for MIL-101(Fe)-NH_2 when the initial concentration of clofibric acid was smaller but as the initial concentration increased, sorption capacity was larger for MIL-101(Fe). Also, the sorption kinetic was much faster towards MIL-101(Fe)-NH_2. Based on the sorption thermodynamics and FT-IR measured after sorption, this phenomenon indicated that sorption towards MIL-101(Fe)-NH_2 was in the form of adsorption. Due to the strong acid-base interaction between the carboxylic group of the clofibric acid and the amine group of MIL-101(Fe)-NH_2, clofibric acid only adsorbed on to the surface of MIL-101(Fe)-NH_2 rather than entering the inside of its pores. Furthermore, the forms of clofibric acid and MIL-101(Fe)-NH_2 changed depending on the pH. At pH in between 3.18 to 4.5, electrostatic interaction was another interaction formed between MIL-101(Fe)-NH_2 and clofibric acid. Hence, the sorption efficiency was highest at pH 4.

Under the irradiation of visible light, clofibric acid was photocatalytically oxidized by the presence of MIL-101(Fe). At the presence of MIL-101(Fe)-NH_2, almost no photocatalytic degradation of clofibric acid was observed. The increasing concentration of 4-chlorophenol during the photocatalytic experiment indicated that clofibric acid was indeed oxidized in the process. However, 4-chlorophenol was not further degraded nor sorbed by MIL-101(Fe) and MIL-101(Fe)-NH_2, being the final product of the photocatalytic oxidation process. The capability of MIL-101(Fe) to serve as photocatalyst stemmed from its bandgap structure. From Tauc method and valence band region of the XPS data, bandgap structure was measured. Having a higher conduction band energy (-0.63 eV) relative to the redox potential of the reduction reaction of oxygen (-0.33 eV), once the electron was excited, superoxide anion radicals could be formed. These superoxide anion radicals could further react with water molecules to form hydroxyl radicals which served as oxidants of clofibric acid. Hence, in MIL-101(Fe), holes could directly oxidize the sorbed clofibric molecules, and the produced hydroxyl radicals could also oxidize both the sorbed and aqueous clofibric acid molecules. Compared to MIL-101(Fe), MIL-101(Fe)-NH_2 did not have the bandgap structure to produce ROS. EPR data showed proof that hydroxyl radicals were formed when using MIL-101(Fe) but did not when MIL-101(Fe)-NH_2 was used.

In this research, the mechanisms for the sorption and photocatalytic degradation of clofibric acid using Fe-based MOFs were expounded. These findings would be helpful in developing novel methods to remove PPCPs from the wastewater.

Reference

Barbosa, A. D. S., Julião, D., Fernandes, D. M., Peixoto, A. F., Freire, C., de Castro, B., Granadeiro, C. M., Balula, S. S., & Cunha-Silva, L. (2017). Catalytic performance and electrochemical behaviour of Metal–organic frameworks: MIL-101(Fe) versus NH2-MIL-101(Fe). *Polyhedron*, *127*, 464–470.

Bedia, J., Muelas-Ramos, V., Peñas-Garzón, M., Gómez-Avilés, A., Rodríguez, J. J., & Belver, C. (2019). A review on the synthesis and characterization of metal organic frameworks for photocatalytic water purification. In *Catalysts* (Vol. 9, Issue 1). MDPI AG.

Bezverkhyy, I., Weber, G., & Bellat, J. P. (2016). Degradation of fluoride-free MIL-100(Fe) and MIL-53(Fe) in water: Effect of temperature and pH. *Microporous and Mesoporous Materials*, *219*, 117–124.

Chen, P., Wang, F., Zhang, Q., Su, Y., Shen, L., Yao, K., Chen, Z. F., Liu, Y., Cai, Z., Lv, W., & Liu, G. (2017). Photocatalytic degradation of clofibric acid by g-C3N4/P25 composites under simulated sunlight irradiation: The significant effects of reactive species. *Chemosphere*, *172*, 193–200.

De Vos, A., Hendrickx, K., Van Der Voort, P., Speybroeck, V. Van, & Lejaeghere, K. (2017). *Missing Linkers: An Alternative Pathway to UiO-66 Electronic Structure Engineering*.

Dong, Y., Hu, T., Pudukudy, M., Su, H., Jiang, L., Shan, S., & Jia, Q. (2020). Influence of microwave-assisted synthesis on the structural and textural properties of mesoporous MIL-101(Fe) and NH2-MIL-101(Fe) for enhanced tetracycline adsorption. *Materials Chemistry and Physics*, *251*, 123060.

Gao, Y., Yu, G., Liu, K., Deng, S., Wang, B., Huang, J., & Wang, Y. (2017). Integrated adsorption and visible-light photodegradation of aqueous clofibric acid and carbamazepine by a Fe-based metal-organic framework. *Chemical Engineering Journal*, *330*, 157–165.

Hasan, Z., Choi, E. J., & Jhung, S. H. (2013). Adsorption of naproxen and clofibric acid over a metal–organic framework MIL−101 functionalized with acidic and basic groups. *Chemical Engineering Journal*, *219*, 537–544.

Hasan, Z., & Jhung, S. H. (2015). Removal of hazardous organics from water using metal−organic frameworks (MOFs): Plausible mechanisms for selective adsorptions. *Journal of Hazardous Materials*, *283*, 329–339.

He, J., Zhang, Y., Zhang, X., & Huang, Y. (2018). Highly efficient Fenton and enzyme−mimetic activities of NH2−MIL−88B(Fe) metal organic framework for methylene blue degradation. *Scientific Reports*, *8*(1), 5159.

He, L., Dong, Y., Zheng, Y., Jia, Q., Shan, S., & Zhang, Y. (2019). A novel magnetic MIL−101(Fe)/TiO2 composite for photo degradation of tetracycline under solar light. *Journal of Hazardous Materials*, *361*(May 2018), 85–94.

He, Y. C., Yang, J., Kan, W. Q., Zhang, H. M., Liu, Y. Y., & Ma, J. F. (2015). A new microporous anionic metal−organic framework as a platform for highly selective adsorption and separation of organic dyes. *Journal of Materials Chemistry A*, *3*(4), 1675–1681.

Horiuchi, Y., Toyao, T., Miyahara, K., Zakary, L., Van, D. Do, Kamata, Y., Kim, T. H., Lee, S. W., & Matsuoka, M. (2016). Visible−light−driven photocatalytic water oxidation catalysed by iron−based metal−organic frameworks. *Chemical Communications*, *52*(29), 5190–5193.

Kraut, E. A., Grant, R. W., Waldrop, J. R., & Kowalczyk, S. P. (1980). Precise Determination of the Valence−Band Edge in X Ray Photoemission Spectra. *Physical Review Letters*, *44*(24), 1620.

Lapworth, D. J., Baran, N., Stuart, M. E., & Ward, R. S. (2012). Emerging organic contaminants in groundwater: A review of sources, fate and occurrence. In *Environmental Pollution* (Vol. 163, pp. 287–303). Elsevier.

Laurier, K. G. M., Vermoortele, F., Ameloot, R., De Vos, D. E., Hofkens, J., & Roeffaers, M. B. J. (2013). Iron(III)-based metal-organic frameworks as visible light photocatalysts. *Journal of the American Chemical Society*, *135*(39), 14488–14491.

Liu, R., Chi, L., Wang, X., Wang, Y., Sui, Y., Xie, T., & Arandiyan, H. (2019). Effective and selective adsorption of phosphate from aqueous solution via trivalent-metals-based amino-MIL-101 MOFs. *Chemical Engineering Journal*, *357*, 159–168.

Nie, Y., Deng, S., Wang, B., Huang, J., & Yu, G. (2014). Removal of clofibric acid from aqueous solution by polyethylenimine-modified chitosan beads. *Frontiers of Environmental Science and Engineering*, *8*(5), 675–682.

Ramalho, M. L. A., Madeira, V. S., Brasileiro, I. L. O., Fernandes, P. C. R., Barbosa, C. B. M., Arias, S., & Pacheco, J. G. A. (2021). Synthesis of mixed oxide Ti/Fe2O3 as solar light-induced photocatalyst for heterogeneous photo-Fenton like process. *Journal of Photochemistry and Photobiology A: Chemistry*, *404*(April 2020).

Shen, K., Chen, X., Chen, J., & Li, Y. (2016). Development of MOF-Derived Carbon-Based Nanomaterials for Efficient Catalysis. *ACS Catalysis*, *6*(9), 5887–5903.

Wang, D., Jia, F., Wang, H., Chen, F., Fang, Y., Dong, W., Zeng, G., Li, X., Yang, Q., & Yuan, X. (2018). Simultaneously efficient adsorption and photocatalytic degradation of tetracycline by Fe-based MOFs. *Journal of Colloid and Interface Science*, *519*, 273–284.

Zhang, C., Ai, L., & Jiang, J. (2015). *Solvothermal synthesis of MIL-53(Fe) hybrid magnetic composites for photoelectrochemical water oxidation and organic pollutant photodegradation under visible light †*.

Zhang, Z., Li, X., Liu, B., Zhao, Q., & Chen, G. (2016). Hexagonal microspindle of NH2-MIL-101(Fe) metal-organic frameworks with visible-light-induced photocatalytic activity for the degradation of toluene. *RSC Advances*, *6*(6), 4289–4295.

초 록

철 기반 금속유기골격체를 이용한 clofibric acid의 흡착 및 광분해 기작

서울대학교 대학원
건설환경공학부
채승희

의약품 및 개인위생용품 (pharmaceutical and personal care products; PPCPs) 물질은 목적에 맞게 사용된 후에 폐수에 유입되며, 폐수처리장에서 모두 분해되지 못하고 방출된다. 하지만 아직 PPCPs의 유해성 및 처리방침이 규명되지 않았으므로 그에 대한 해결책이 요구된다. 위 연구에서는 PPCPs에 해당하는 clofibric acid를 대표오염물질로 선정하였고 이를 수계에서부터 제거할 수 있는 방법을 제시하고자 하였다. 다양한 방법 중 흡착시킨 후 광촉매 기작을 통해 분해까지 하는 제거방법은 에너지 효율 측면에서 주목받고 있는데, 해당 연구에서는 이를 위하여 흡착과 광촉매가 모두 가능한 금속유기골격체 (metal organic framework; MOF)를 사용하였다. 그 중에서도 철을 중심금속으로 하는 MOF를 사용하여 광촉매 특성을 갖추도록 하였다. 또한, 동일한 유기리간드에 추가적으로 아민기가 부착된 유기리간드를 사용하여 최종적으로 MIL-101(Fe)와 MIL-101(Fe)-NH_2를 이용하여 clofibric acid에 대한 흡착 및 광촉매 기작 특성을 규명하고자 하였다.

합성한 MIL-101(Fe)와 MIL-101(Fe)-NH_2의 구조적 및 화학적 특성을 FE-SEM, XRD, FT-IR을 활용하여 분석한 결과, 두

MOF 모두 결정질 구조를 갖추고 있었으며 표면에 카르복실기와 아민기에 해당하는 작용기를 지니고 있었다. 특히, 두 MOF 모두 1006, 848 m^2/g의 BET 표면적을 지녀 흡착제로 사용되기 적합함을 보여주었다.

두 MOF를 이용하여 clofibric acid를 흡착한 결과, 50 mg/L 이하의 초기농도 조건에서는 MIL-101(Fe)-NH_2을 사용하였을 때 흡착 효율이 더 높았지만 초기농도가 증가함에 따라 MIL-101(Fe)의 흡착 효율이 더 높아졌다. 또한 흡착 kinetic을 살펴본 결과, 모든 초기농도 조건에 대해서 MIL-101(Fe)-NH_2을 사용했을 때의 kinetic constant가 항상 더 컸다. 더 나아가 sorption thermodynamics와 흡착 전후의 FT-IR 결과에 따라 MIL-101(Fe)-NH_2의 흡착은 주로 adsorption의 형태로 이루어짐이 밝혀졌다. 특히, MOF의 아민기와 clofibric acid의 카르복실기 간의 강한 산 염기 상호작용에 의해 clofibric acid가 MOF의 표면에 주로 흡착하며 MOF의 공극 내로는 이동하지 않음을 추측할 수 있었다. 더 나아가, 용액의 pH가 변함에 따라 흡착 기작이 변함을 알 수 있었는데, pH가 3.18에서 4.5 사이 일 때는 카르복실기가 음전하를, 아민기가 양전하를 띰에 따라 정전기적 인력에 의해 강한 흡착이 발생함을 알 수 있었다. 결과적으로, pH가 4일 때 가장 높은 흡착 효율을 지님을 확인했다.

흡착이 진행된 후에 용액에 가시광선을 쪼이면 clofibric acid가 MIL-101(Fe)의 광촉매 기작에 의해 분해됨을 확인했다. 반면, MIL-101(Fe)-NH_2를 사용했을 경우에는 흡착에 의해서 clofibric acid가 용액으로부터 제거되긴 했으나 흡착된 clofibric acid의 분해는 거의 이루어지지 않았다. 더 나아가, clofibric acid의 산화반응에 대한 결과물로 4-chlorophenol이 검출되는 것을 확인했지만 이는 MIL-101(Fe), MIL-101(Fe)-NH_2 모두에 대해 흡착되지도, 분해되지도 않아 해당 실험의 최종 결과물로 확인되었다. MIL-101(Fe)의 광촉매 기작을 분석하기 위해 Tauc method와 해당 물질의 XPS 결과의

valence band region으로부터 bandgap energy 구조를 규명했다. 그 결과, MIL-101(Fe)의 경우에는 conduction band energy가 -0.63 eV로 산소의 환원반응에 필요한 환원전위인 -0.33 eV보다 높았다. 즉, MIL-101(Fe)가 광촉매 기작에 의해 전자의 여기(excitation)가 발생하면 여기된 전자에 의해 용액의 용존 산소가 superoxide anion radical로 환원이 가능했다. superoxide anion radical은 물 분자와 반응하여 hydroxyl radical이 생산되며, 생산된 hydroxyl radical은 흡착되어 있는 clofibric acid 및 용존 clofibric acid를 산화시킬 수 있었다. 또한, 전자가 여기된 후에 생긴 valence band의 hole에 의해서 흡착된 clofibric acid의 직접 산화반응이 발생가능했다. MIL-101(Fe)과는 달리 MIL-101(Fe)-NH_2의 conduction band energy가 0.08 eV로 활성산소종을 발생시킬 수 없는 bandgap 구조를 지니고 있어 오직 valence band에 생긴 hole에 의한 clofibric acid의 직접 산화반응만이 광분해에 기여했다. 해당 광촉매 기작은 EPR 결과를 통해 MIL-101(Fe)는 가시광선에 노출되었을 때 hydroxyl radical을 생산한 반면, MIL-101(Fe)-NH_2는 발생시키지 못함을 확인하여 추가적으로 입증되었다.

해당 연구를 통해 MIL-101(Fe)와 MIL-101(Fe)-NH_2를 사용하여 clofibric acid에 대한 흡착 및 광촉매 분해 기작을 규명하였다. 위 연구의 결과를 통해 광에너지와 같은 재생에너지를 사용하여 폐수에 포함된 PPCPs를 제거하는 차세대 기술 개발에 기여할 것으로 기대된다.

주요어 : 금속유기골격체, 의약품 및 개인위생용품, 흡착, 광촉매, 수질오염물질
학 번 : 2019-24759